

Measurement and Modeling of Oxide Inclusions in Steel Casting: Production Casting Case Study

Richard A. Hardin and Christoph Beckermann

Department of Mechanical Engineering

The University of Iowa, Iowa City, 52242

Abstract

A case study investigating inclusions in a production steel casting is presented. Castings were poured at a Steel Founders' Society of America (SFSA) member foundry. The castings had two rigging/gating configurations. Four castings were produced using a bottom filling gating system (so-called naturally pressurized gating), and three were poured directly into a feeder without any gating system. The objective of the case study was to compare the inclusion inspection results and simulation predictions from the two rigging cases. The results of the inclusion measurements made on the castings' surface were analyzed to determine if there were differences in the area coverage of inclusions on the casting surfaces. On average the bottom-filled castings had 0.4% and the feeder-filled had 2.2% inclusion area coverage on the casting cope surfaces. The observed inclusion locations on the surfaces were not repeatable for either gating system. The measured inclusion area coverage for the seven castings were compared to simulation results. The simulations use a model where the local air entrainment rate is calculated from disturbances at the free surface of the filling flow. Results of the air entrainment model are used to generate oxide inclusions at the locations of air entrainment during filling. The model predicts the formation, transport and final locations of oxide inclusions in the castings system generated by air entrainment. Measured and simulated inclusion area, count, and size are compared to determine the modeling parameters giving the best agreement with the measurements. Using the best model parameters, the predicted and measured inclusion area fractions on the cope surfaces of the castings are 0.36% and 0.4%, respectively, for the cases with gating. The predicted and measured inclusion area fractions on the cope surfaces of the castings without gating are 1.83% and 2.16%, respectively. The percentage difference between the predictions and measurements for these cases are 9.5% with gating and 15.2% for the feeder-filled case.

1. Introduction

Oxide inclusions in steel castings are estimated to contribute 20% to the cost of a casting due to the costs of removing them and repairing the casting [1]. They are also a frequent cause of premature failure of steel castings when not detected during production. There are numerous sources of oxides such as the ladle lining and poorly deoxidized melt, and many casting process variables can affect the levels of oxides in steel castings. The cleanliness of the melt can vary from heat to heat, so called dirty heat versus clean heat, due to lack of control of the melt practice. Considering all the sources of oxide inclusions, reoxidation inclusions, formed during pouring of the metal into the mold, are a common cause of inclusion defects in steel castings, if not the most

common. Reoxidation inclusions form when deoxidized steel comes into contact and reacts with oxygen during mold filling. They are reported to make up 83% of oxide inclusions in low-alloy steel castings and 48% of inclusions found in high-alloy steel castings [2]. Reoxidation of the steel during pouring can be minimized by employing well designed gating systems. Much research has been performed for over 50 years to establish rules for gating castings. However, the design of gating systems is still both an art and a science.

Air entrainment during mold filling is the main source of the oxygen that is consumed in reoxidation inclusion formation. For many decades air entrainment at the air-water interface of free surface flows has been an important research topic in hydraulics and multiphase fluid mechanics. Two reviews documenting the scope and progress of experimental and computational air entrainment research are presented by Chanson [3,4]. In free surface flows, air is entrained at surface discontinuities. Such surface discontinuities are created, for example, by a liquid jet plunging into a pool (as shown in Figure 1), breaking waves, or a hydraulic jump, in which a fast-

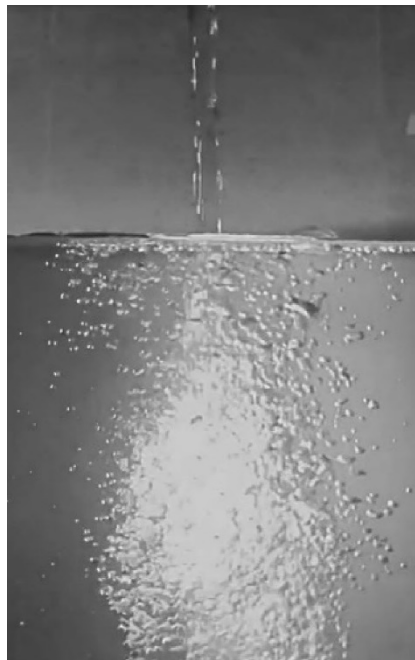


Figure 1. Air entrainment by a plunging water jet into a quiescent pool. Bubbles form at the perimeter of the jet's intersection with the pool.

moving liquid discharges into a low velocity atmosphere. In the plunging jet case, the air is entrained in a thin layer around the perimeter of the jet where it enters the pool. The air entrainment rate depends primarily on the jet velocity, diameter and turbulence level. Air entrainment commences only above a certain critical jet velocity (approximately 1 m/s for water). For water jet velocities at the point of impact of the order of 5 m/s, the relative air entrainment (V_a/V_s) of one cubic meter of air (V_a) per cubic meter of water flowing (V_s) are easily reached.

During mold filling, free surface flows can occur that entrain air. Liquid metal plunging into

the sprue, jets emanating from ingates or falling over edges inside of the casting cavity and returning waves in runners are some of the most important examples of such flows. The oxygen in entrained air reacts almost immediately with elements in the liquid steel to form solid, liquid, and/or gaseous oxides. While the gaseous oxides can often escape from the casting cavity, liquid and solid oxides are transported with the liquid metal and ultimately end up as non-metallic inclusions in the solidified casting.

In steel casting, the inclusions are always lighter than the metal and often accumulate on the cope surface. For a typical inclusion composition in steel, Figure 2 shows the inclusion volume fraction (volume of inclusions to volume of steel ratio, V_{inc}/V_s) as a function of the relative air entrainment [5]. As indicated by the vertical dashed line in Figure 2, a relative air entrainment (V_a/V_s) of about 3.5 cubic feet of air (at ambient temperature and pressure) per cubic foot of steel, which is easily reached, results in one cubic inch of inclusions per cubic foot of steel.

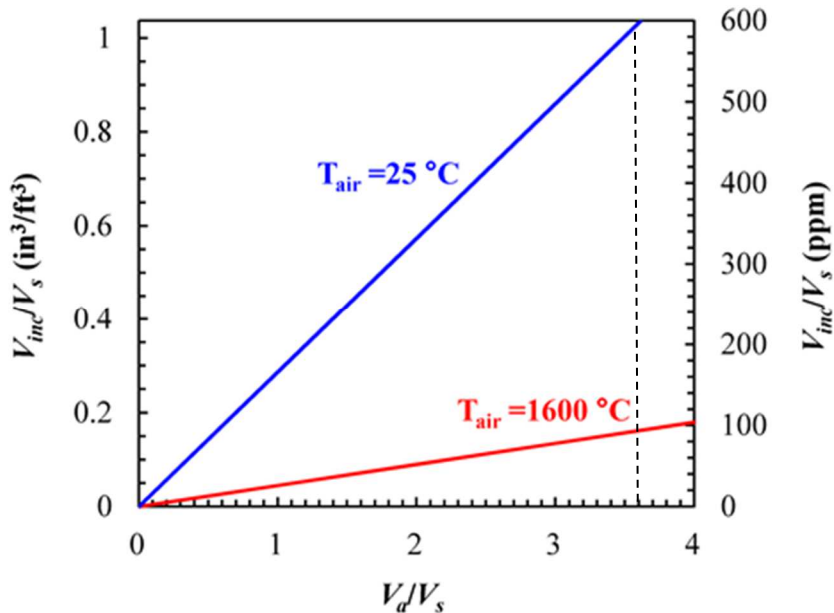


Figure 2. Variation of inclusion volume fraction with relative air entrainment for carbon/low-alloy steel [5].

The air entrainment model used to generate inclusions in this case study has been published in the open literature so that any casting software developers can implement it in their software [6]. The air entrainment model was further developed to generate inclusions locally in the simulation where air entrainment occurs. After the inclusions form, they are transported by the filling flow to their final locations. The inclusions are transported using the inclusion motion model presented in [7]. The air entrainment and inclusion models have been implemented in casting simulation software available to the industry [8] so this research can be transitioned to industrial applications.

Turbulence plays an important role in air entrainment and the generation of inclusions in filling steel castings. Turbulence can be introduced during filling by throttling the inlet flow, for example. Consider the plunging jet shown in Figure 1. The turbulence level of the plunging jet on the relative air entrainment rate was investigated experimentally by Ervine et al. [9]. The turbulence intensity for a plunging jet is defined as

$$I = \frac{\sqrt{u'^2}}{\bar{u}} \quad (1)$$

where u is the velocity of the jet, and the prime and the overbar indicate the fluctuating and mean components of the velocity, respectively. In [9], turbulence was induced by applying the following time-dependent sinusoidal velocity profile at the inlet stream

$$u = \bar{u} + u' = \bar{u} [1 + I \times \sin(\omega t)] \quad (2)$$

where ω and t are frequency and time, respectively. In the experimental study by Ervine et al. [9], the frequency was set to $\omega = 65\pi$ and the turbulence intensity to $I = 0.05 = 5\%$. Simulations were performed for four different mean jet velocities [6] using the air entrainment model applied in this inclusion case study. The results as shown in Figure 3 give good agreement between the

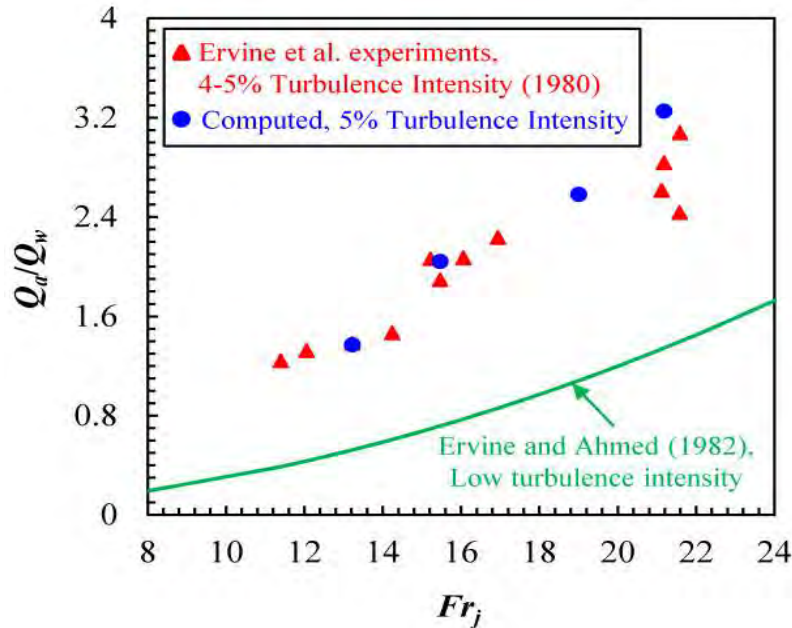


Figure 3. Comparison between measured and predicted relative air entrainment rates for a turbulent plunging jet with and without turbulence.

measured and predicted relative air entrainment rates versus Froude number for a turbulent plunging jet. In this figure Q_a is the air entrainment rate, Q_w is the jet flow rate, and the Froude number is defined

$$Fr_j = \sqrt{\frac{u_j^2}{gd_j}} \quad (3)$$

where u_j is the jet velocity at impact, g is the acceleration due to gravity, and d_j is the jet diameter at impact. For a turbulence intensity of 5%, the relative air entrainment rate increases for the simulations and measurements by a factor of approximately three relative to the low turbulence correlation curve as determined by Ervine and Ahmed [10] (shown by the green curve in Figure 3). Clearly, turbulence is an important variable in air entrainment.

This paper reports on a case study involving production steel castings poured at a Steel Founders' Society of America (SFSA) member foundry. The motivation for the study was to investigate the effect of pouring and gating on the amount and distribution of inclusions on the casting surfaces. Seven castings were poured using two filling configurations. Four castings were poured using a bottom filling gating system (so-called naturally pressurized gating), and three were poured directly into the feeder without a gating system. One objective of the case study was to compare the inclusion inspection results for the two rigging cases. The results of the inclusion measurements made on the castings' surface were analyzed to determine if there were differences in the observed amount of inclusions on the casting surfaces. The inclusion locations on the surfaces were analyzed to see if final inclusion locations were repeatable or different between the two types of gating systems. Another objective of the study was to compare measured and simulated inclusion distributions and quantitative amounts on the casting surfaces. In these comparisons, the inclusion area percent coverage on the casting cope surfaces were analyzed. Also, the simulated and observed inclusion count (or number) and mean diameter were compared for casting cope surfaces. A parametric study of the effects of modeling variables on the simulation results was also performed as summarized below.

2. Procedures Used in Casting, Inclusion Measurement and Modeling

2.1 Casting and Inclusion Inspection Procedures

The casting selected for this case study was the so-called "platypus" casting which is shown as the gray object in Figure 4. The platypus casting is specified as part of a qualification process for foundries to produce castings for the United States Navy. Four of the castings were poured using a bottom filling gating system which is shown in Figure 4(a) with a dimension given to scale the casting size, and three were poured directly into the feeder without a gating system shown in Figure 4(b). Note as shown in Figure 4 that six tapered cylindrical vents were used and modeled for each casting system. The weight of metal poured for the bottom filled casting system was 420 pounds, and the weight poured for the feeder filled casting system was 337 pounds. The alloy poured was AISI 8630. The average pouring time for the bottom-filled casting was 14.0 seconds, and 12.6 seconds for the feeder-filled casting. The castings were poured from a 20 ton bottom-pour ladle with a nozzle having a 2.5" diameter opening.

Inclusion inspection was performed at the foundry. After the castings were poured, cooled and shaken out of their sand molds, the castings' surfaces were cleaned using an angle grinder with a wire wheel brush. Then the inclusion locations were marked using water soluble liquid chalk pens.

Photographic images were made from all directions of the inspected and marked-up casting surfaces. Images of the views were made multiple times to obtain the best lighting and exposures possible. The inclusion distributions from the inspection images were measured and analyzed later using image analysis software.

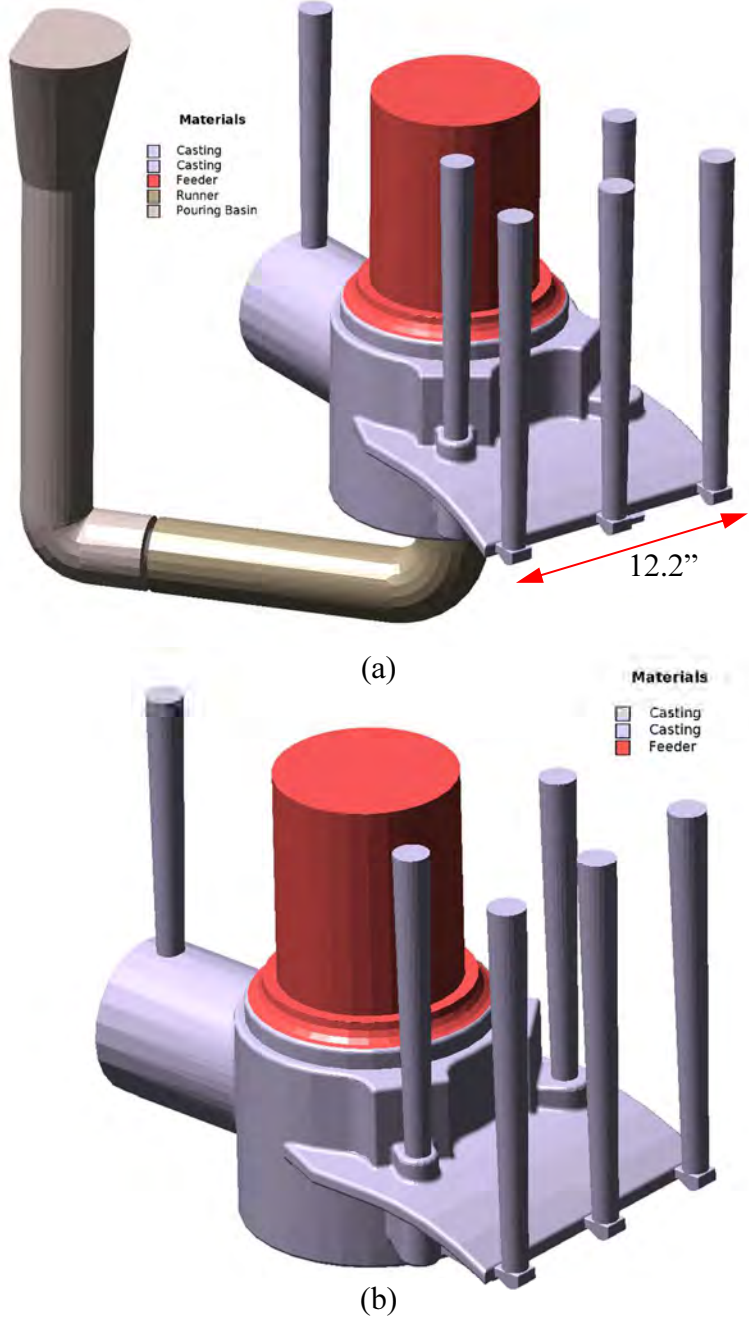


Figure 4. Solid model of the bottom-filled castings and rigging (a) and model of castings poured through the feeder without a gating system (b).

An image of one of the bottom-filled casting is shown in Figure 5(a) before cleaning using wire brushing showing the drag (bottom facing) side with the two ends (tail and bill) labeled. This terminology is used with reference to the flat curved surface resembles a platypus bill, so the cylinder feature is referred to as the tail end. The castings were cleaned by wire brushing and the



(a)



(b)

Figure 5. Photo of a bottom-filled casting (a) before cleaning using wire brushing showing the drag (bottom facing) side with the two ends (tail and bill) labeled. Photo of the lighting setup (b) used at the foundry to photograph the castings with marked up inclusion indications.

vents shown in Figure 5(a) were removed. A fork lift was used to position the castings for marking up the inclusions and then photographing them. A photo of the lighting setup used in recording images of the castings with marked up inclusion indications for one of the bottom-filled castings is shown in Figure 5(b)

Two types of surface indications were marked on the casting surfaces. Indications marked in yellow were areas and locations identified with inclusions. Indications marked in blue were identified by the foundry personnel as de-oxidation by-products, and these appeared as white deposits on the casting surface. In Figure 6 photos of the cope surface at the bill end of two marked



(a)



(b)

Figure 6. Photos of the cope (top) surfaces of the “bill” ends with indications marked up for (a) a casting filled through the feeder and (b) a bottom-filled casting using a gating system.

up castings are shown. The yellow and blue indications marked up on a casting filled through the feeder are shown in Figure 6(a) and the marked-up surface of a bottom-filled casting is shown in Figure 6(b). In Figure 7 photos of the cope surface at the tail end of two marked up castings are shown. In this figure indications marked up on a casting filled through the feeder are shown in Figure 7(a), and the marked-up surface of a bottom-filled casting is shown in Figure 7(b). In general, the bottom-filled castings had cleaner casting surfaces than the castings filled through the feeder. This difference in amount of surface indications is noticeable in the case of the castings



(a)



(b)

Figure 7. Photos of the cope (top) surfaces of the “tail” ends with indications marked up for (a) a casting filled through the feeder and (b) a bottom-filled casting using a gating system.

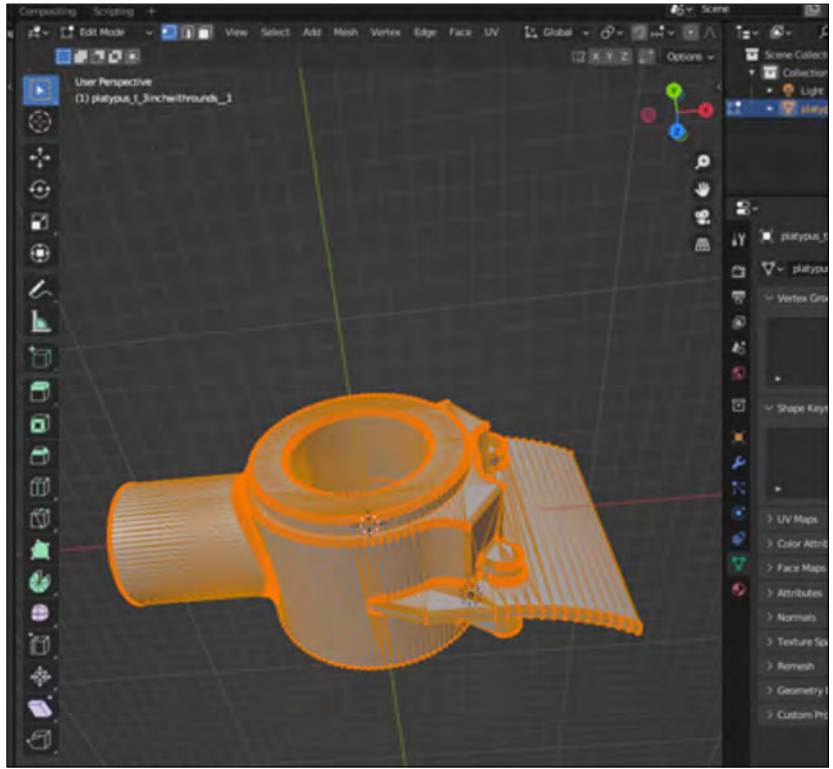
shown in Figure 7. The indications on all casting surfaces were analyzed using images analysis and compared to simulation results as discussed below.

2.2 Transferring Inclusion Images to Models and Image Analysis Procedures

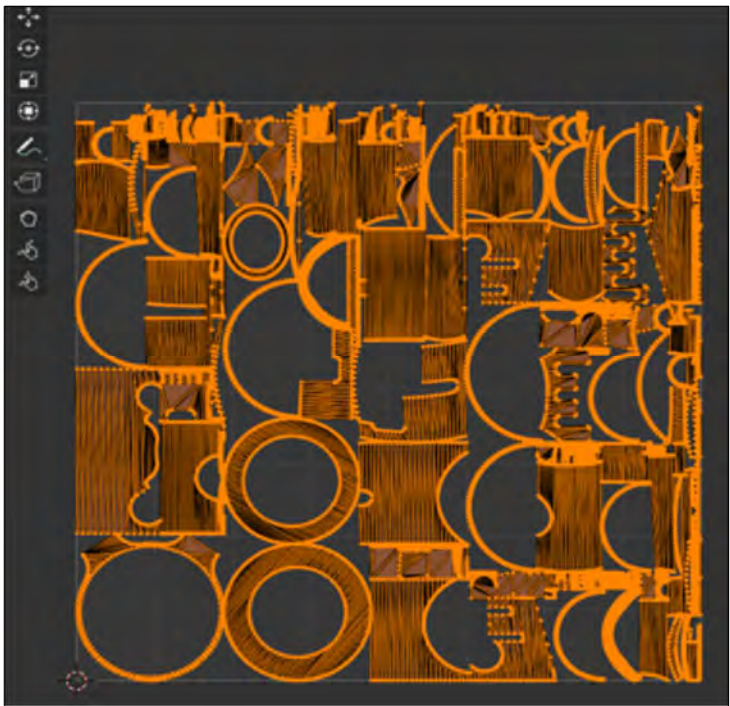
A procedure for transferring information in the photo images of the marked-up inclusions on the casting surfaces to quantitative data describing the inclusion size distribution and locations was developed. This was accomplished using the software *Blender* to transfer the photo image information onto the 3-D casting model, and then to export the 3-D data to 2-D surface information for image analysis. The 2-D surface information for the marked-up inclusions was then analyzed using *ImageJ* software to determine the inclusion size distribution data for a given casting experiment.

The first step in this process is to import a solid 3-D model of the platypus casting into the *Blender* software as shown in Figure 8(a). Next, using the so called “UV mapping” capability in the software, the three-dimensional model surfaces are transformed into 2-D surfaces shown in Figure 8(b). This allows for the accurate mapping of the indications marked in photos of the castings onto the 3-D casting model and then to 2-D images for analysis in the *ImageJ* software. As shown in Figure 9(a) for the top view, indications can be marked onto the 3-D model in any view or perspective. The surface locations on the 3-D model marked-up in Figure 9(a) are identified for the flat “bill” surface marked with a large U-shape, the bosses marked with dots, and the top surface of the bore is marked with a circle. Also drawn is an upturned “smile” on the tail. Essentially a smiley face was drawn on the cope surface of the model. A digital tablet and pen (type XP-Pen Innovator) is used with the *Blender* software to make the digital markings. In Figure 9(b) the resulting 2-D markings on the casting surfaces from the marking in Figure 9(a) are shown. The 2-D surface locations shown in Figure 8(b) are the same as the locations in Figure 9(b). Indications from 2-D binary images exported from *Blender* can be readily analyzed using *ImageJ* software.

To transfer data from the photos of inclusions to the 3-D model in *Blender*, first a transparency is printed from a photo of the marked-up casting like that shown in Figure 10(a). This is an image of the cope surface of the “bill” region for one of the platypus castings with inclusion indications marked in yellow chalk pen. The printed transparency of the image is overlaid onto a scaled and carefully positioned view of the solid model in the *Blender* software as shown in Figure 10(b). The indications marked in yellow on the transparency are then transferred onto the solid model by hand in the *Blender* software through the overlaid printed transparency as shown in Figure 11(a) using the digital pen and tablet. The final result for the marked-up cope 2-D surfaces is shown in Figure 11(b) on the left side and the marked-up solid model cope surface view on the right side in that figure. The image of marked inclusions (Figure 10(a)) is shown in the red box for comparison. Once the entire casting is marked up from the various photographed views of the experiment results, the image of the marked up 2-D surfaces like that shown in Figure 11(b) (on the left side) are saved as an image file. That image file is imported into *ImageJ* and a “particle analysis” is performed on it in that software. The result of this analysis is a table of the indications giving their individual areas and other size and shape data (i.e. circularity, aspect ratio etc.). Results from the image analysis used to evaluate the inclusion distribution measurements were the number of



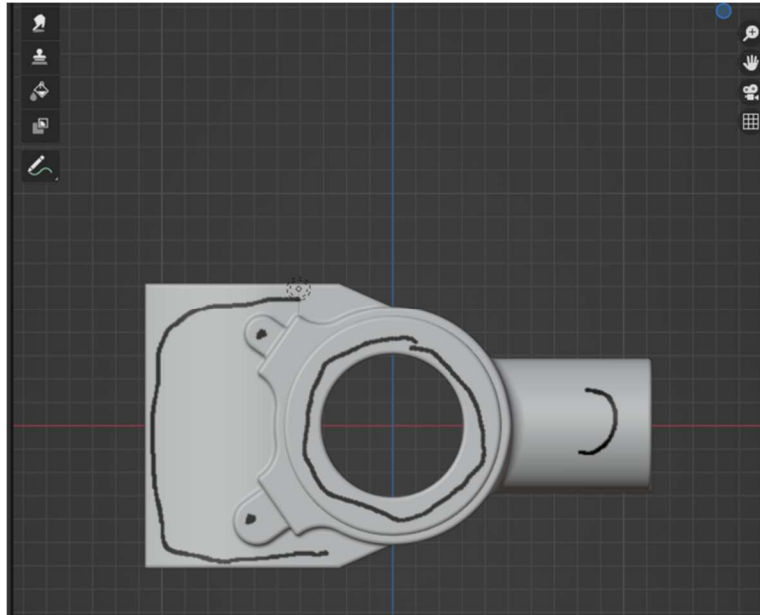
(a)



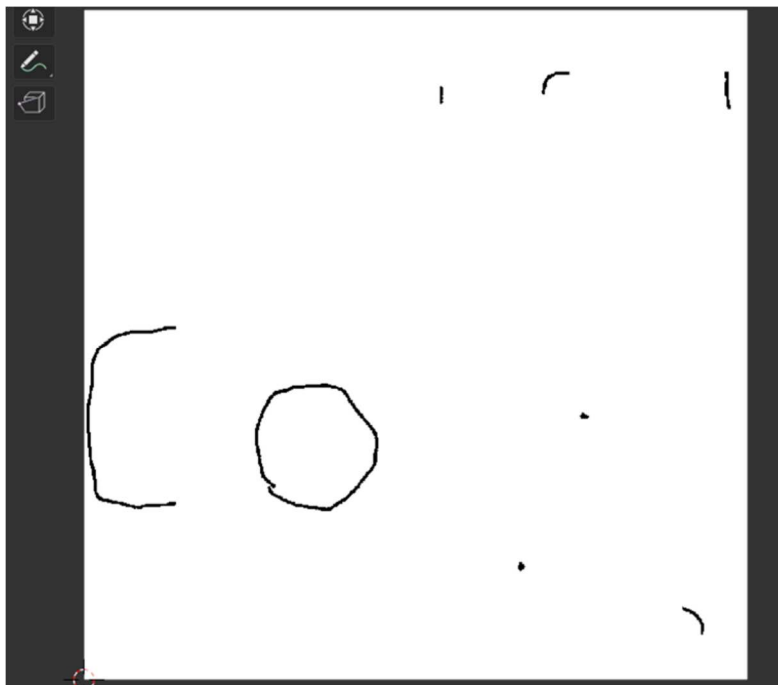
(b)

Figure 8. Solid 3-D model (a) of the platypus casting imported into the *Blender* software, and (b) 2-D surfaces mapped from the 3-D platypus model using the software.

indications, the equivalent diameters of the inclusion indications and the resulting mean diameter. The equivalent diameter is the diameter of a circle having the same area as the area of a given indication. The total area coverage of inclusions on the casting surfaces were also measured from the images. The locations of the inclusions from the experiments can readily be compared to the final simulated inclusion locations as well.



(a)

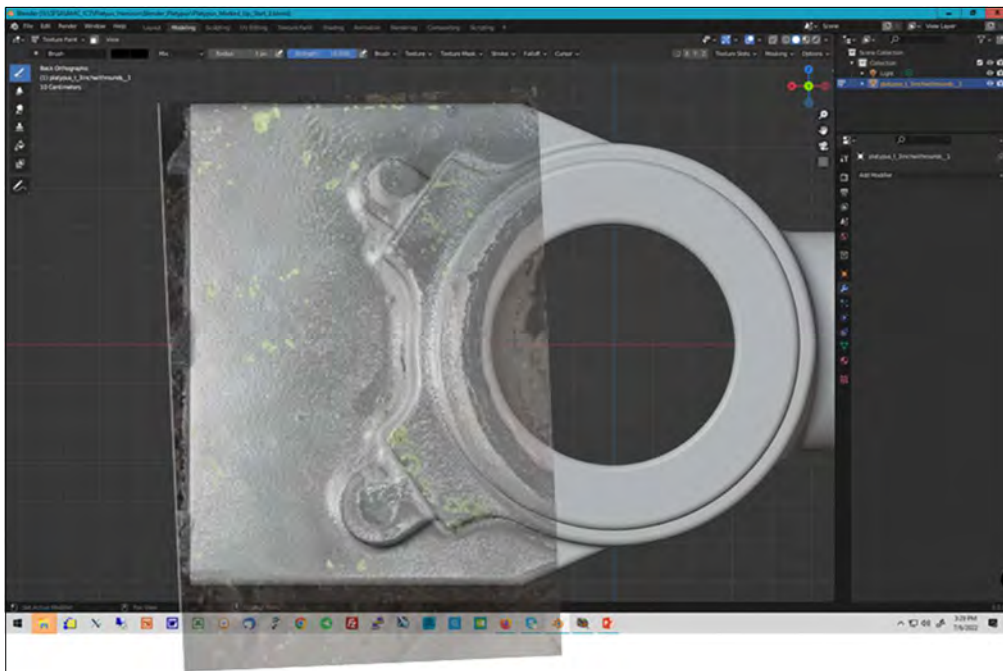


(b)

Figure 9. Marked up cope surface of the 3-D model (a) of the platypus casting in the *Blender* software and marked up 2-D surfaces (b) mapped from the 3-D platypus model using the software.

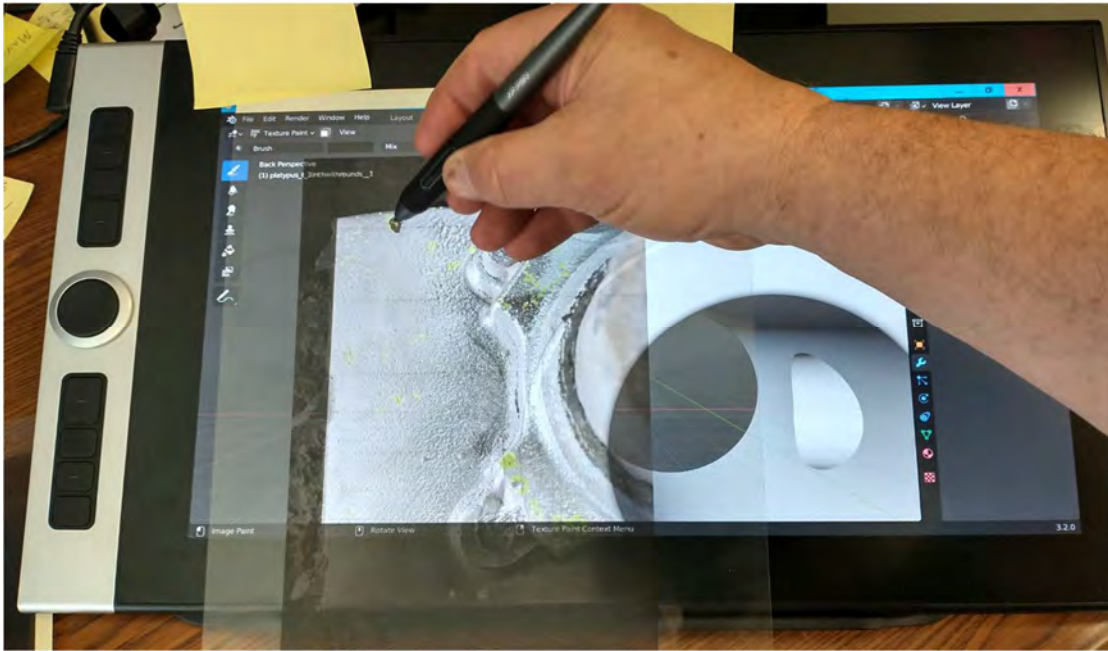


(a)

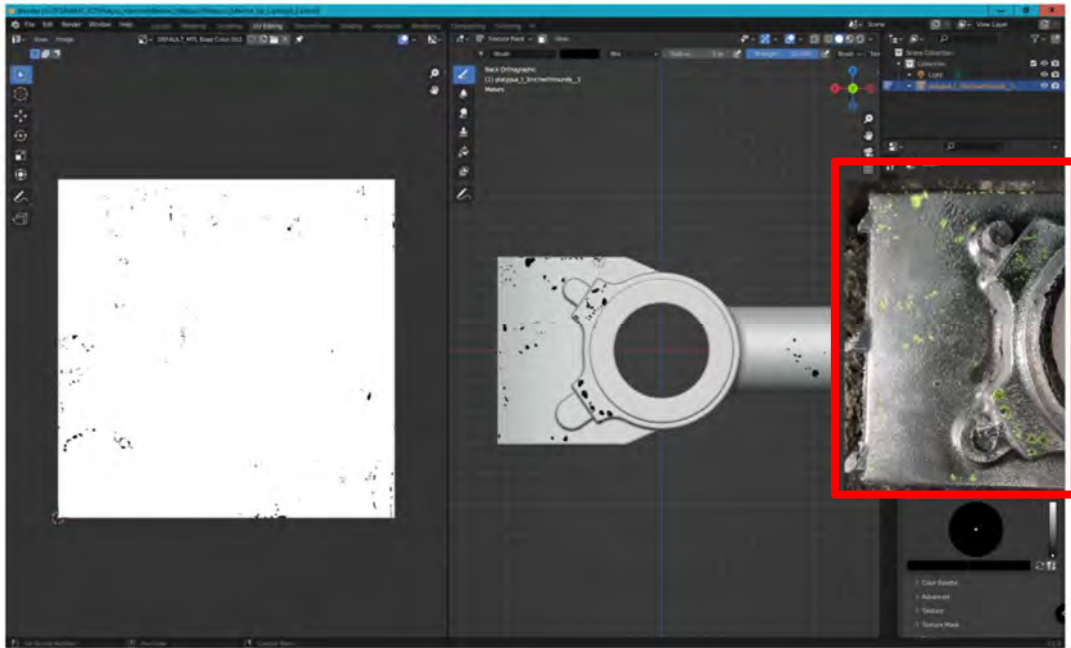


(b)

Figure 10. Image of cope surface of “bill” region (a) for one of the platypus castings with inclusion indications marked in yellow chalk pen. Printed transparency of the image in (a) overlaid onto scaled and onto scaled and positioned view of solid model in the *Blender* software.



(a)



(b)

Figure 11. Marking up the solid model in the *Blender* software (a) through the overlaid printed transparency of the image of marked up inclusions. The result for marked up cope 2-D surfaces (b) on left side and marked up solid model cope surface on right side. Image of marked inclusions is shown in the red box.

In the commercial casting study numbering system, castings numbered 4 through 7 were bottom-filled and castings 8 through 10 were filled by pouring into the feeder. An example of the completed data transfer from the photo images of the marked-up inclusions on the casting surfaces to solid models of the castings is shown in Figure 12 for casting 4. This figure gives views from

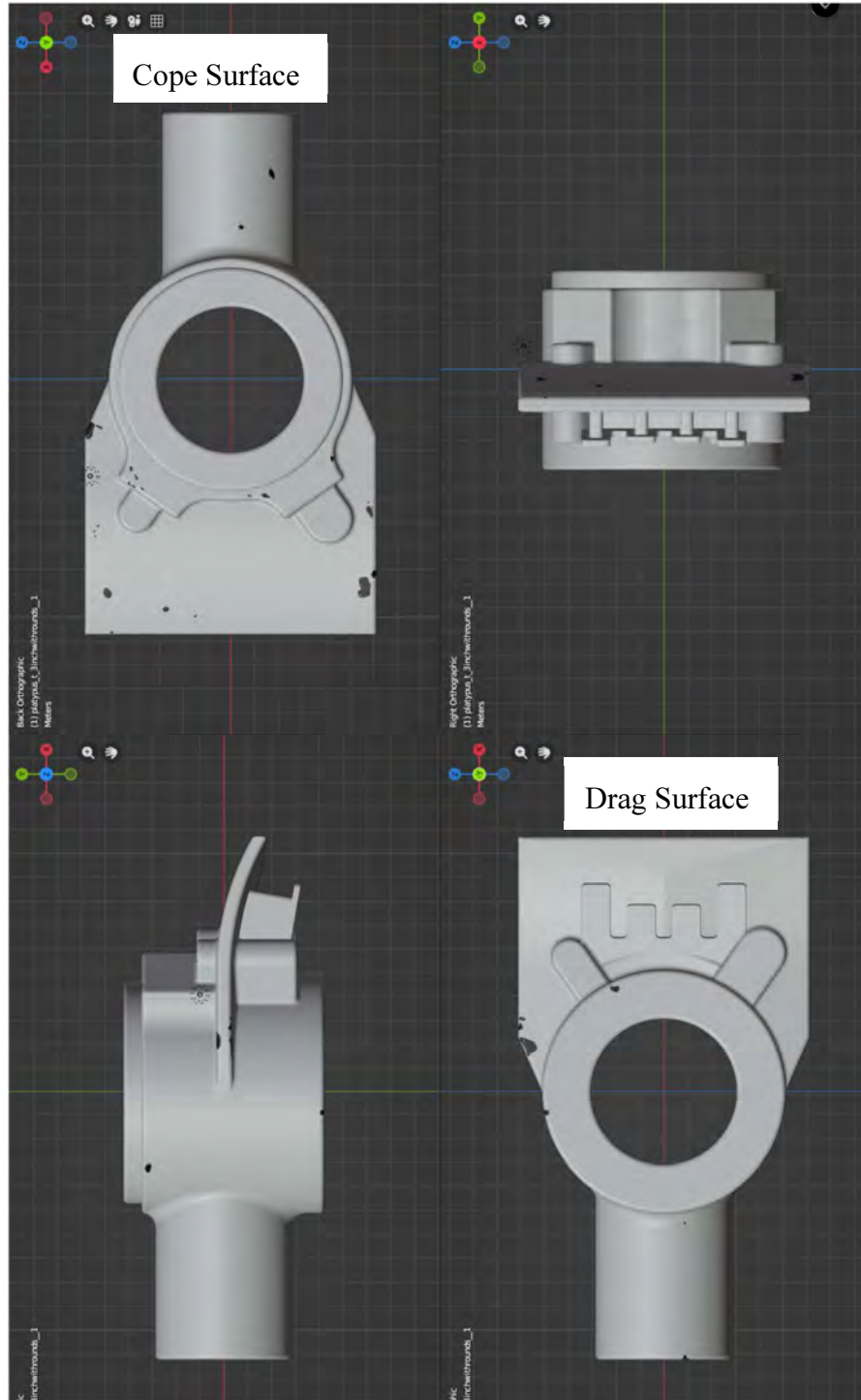


Figure 12. Marked up the solid model for bottom-filled casting 4 poured for the production casting case study in the *Blender* software. Note that the cope (top) and drag (bottom) surface views are indicated. Inclusion areas are indicated in black.

the top (cope surface), bottom (drag surface), and two side views of the marked up solid model in the *Blender* software. An example of an image of the cope surface analyzed after exporting from *Blender* is shown in Figure 13. In this figure the inclusion indication image for the cope surface for casting 4 is given. The black indications are inclusion locations marked on the surfaces that are measured using image analysis in *ImageJ* software. The white area is the casting surface that is free of inclusions. The white and black areas together are the total casting surface area, and the gray area is not included in the analysis. The measurements made using *ImageJ* that are given in the results section of this report are: inclusion area percentage covering the surface, number of discrete inclusion indications, and the mean equivalent diameter of all inclusions.

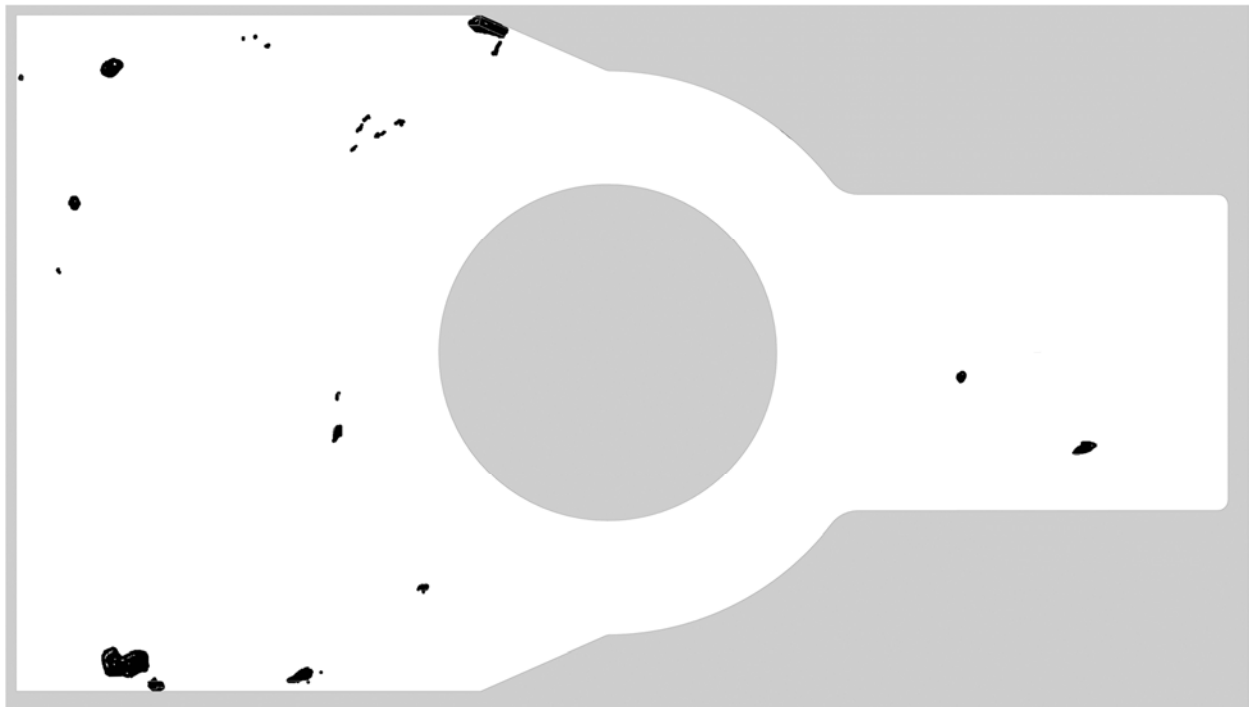


Figure 13. Top view of cope surface area without using shading. Regions marked in black are inclusion indications on cope surface for Casting 4.

2.3 Inclusion Modeling Procedures

Two oxide inclusion modeling approaches were used in this project. Of these, the *Air Entrainment Inclusion Model* was recently developed. This model was implemented in commercial software by our project partner [8]. In this model, inclusions are generated at locations of air entrainment and are transported to their final locations in the casting. Several air entrainment and inclusion model parameters that affect the inclusion generation and transport are discussed below.

The second inclusion model used in this project was developed previously [11], and is referred to as the *Dross Inclusion Model*. The dross inclusion model assumes the source of inclusions is at the inlet to the casting system having (1) a prescribed total number of inclusions N_{inc} entering the

casting system during filling, and (2) a size distribution ranging from 50% to 150% about a prescribed mean inclusion diameter d_{inc} .

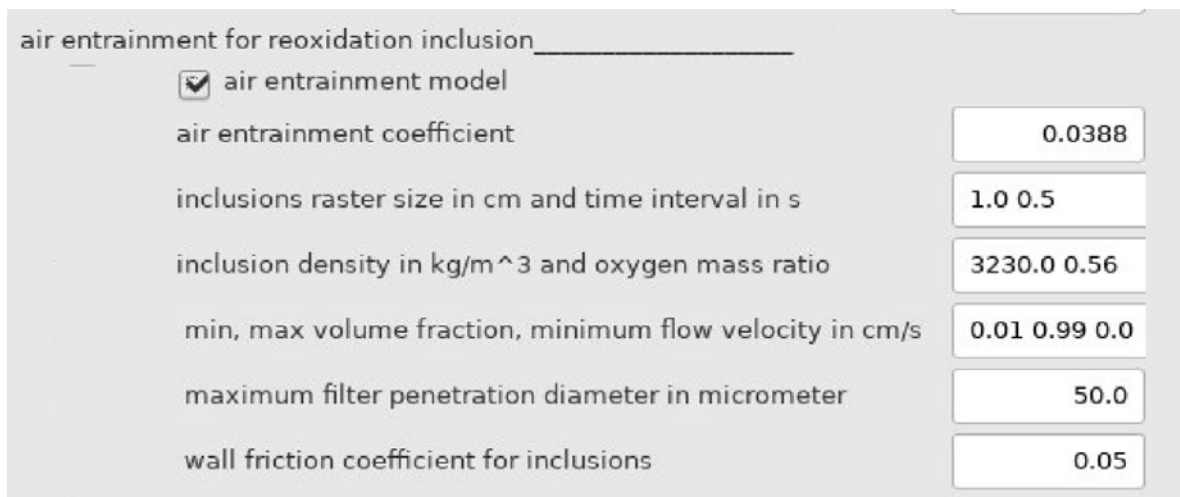
In both models the inclusions are assumed to be spheres. All other aspects of the modeling for calculating the motion and final locations of the inclusions in both inclusion models are as described in [7] and [11]. Additional parameters used in the inclusion equation of motion in both inclusion models are the inclusion density ρ_{inc} and the wall slip coefficient λ_{inc} . The two inclusion models may be used independently or in combination. The results from both models can be analyzed to determine the amount of area coverage and final locations of oxide inclusions in steel castings.

Images of the simulation results are generated that are analogous to Figure 13, and these are analyzed in the same way as the experimental results. However, to compare the simulation results to the experiments, the inclusion simulation results must be quantitatively evaluated to determine the inclusion area coverage and inclusion number on the casting surfaces. The inclusions on the experiment casting surfaces are observed to be pancake-shaped, while the inclusions formed in the simulations are spheres. To make the comparison to the measurements, the spherical inclusions on the surfaces of the simulated castings are converted to flattened disks having the same volume. A flattened inclusion has a larger diameter than a sphere of the same volume. Based on an experimental study of inclusions removed from the surfaces of castings, it was found that the actual flattened inclusions had an average diameter 1.7 times the diameter of a sphere having the same volume. To analyze the simulated inclusion size distributions, an image of the inclusion distribution result on the surface analyzed is made in the software's post-processor with the inclusions scaled to their true size. To model the flattened shape of the inclusions observed in the experiments, these spherical results are converted to flat disk diameters by increasing their size using a factor of 1.7 in the software's post-processor. Then the image of the flattened inclusions is converted to a binary image and analyzed using the software *ImageJ*. As with the measured inclusion images, the particle analysis feature in *ImageJ* is used to calculate the inclusion area coverage on the casting surface, inclusion count/number and the average diameter from the simulation results.

Since the air entrainment inclusion model was developed recently for this study, it will be discussed here for the first time in detail. As shown in Figure 14 by an image taken from the software's user preferences interface, key air entrainment inclusion model parameters have been added for this inclusion model. These include:

- 1) The air entrainment coefficient, which drives the volume of air entrained. It has a default value of 0.0388 currently.
- 2) The inclusion density that affects their transport. It has a default value of 3230 kg/m³.
- 3) The wall sticking coefficient which contributes to the inclusion particle transport and the final inclusion locations. It has a default value of 0.05.
- 4) Oxygen mass ratio (OMR) - This is the ratio of oxygen mass in reoxidation inclusion to its total mass. It depends on the chemical composition of the inclusion. If the mass ratio is larger it takes a larger amount of O₂ to generate a given amount of inclusion mass. Therefore

- a larger mass ratio generates less inclusion mass for the same amount of entrained oxygen. OMR drives the mass and size of inclusions generated and currently its default value is 0.56.
- 5) Inclusion raster size (cm) – This is the spatial length over which inclusions form. A larger raster size increases the inclusion size, but results a smaller number of inclusions. The total mass of inclusions generated is conserved.
 - 6) Inclusion time raster interval (s) – This is the time interval over which inclusions form. A longer time interval allows larger inclusions to form but creates fewer of them. Again, the total mass of inclusions generated is conserved.
 - 7) For the inclusion filtering model, the filter critical diameter is used in filter applications. Inclusion particles having a diameter greater than the critical diameter are trapped by the filter. So if it is 0 all inclusions are trapped by the filter, and if very large all inclusions pass through filter.



Parameter	Value
air entrainment model	<input checked="" type="checkbox"/>
air entrainment coefficient	0.0388
inclusions raster size in cm and time interval in s	1.0 0.5
inclusion density in kg/m ³ and oxygen mass ratio	3230.0 0.56
min, max volume fraction, minimum flow velocity in cm/s	0.01 0.99 0.0
maximum filter penetration diameter in micrometer	50.0
wall friction coefficient for inclusions	0.05

Figure 14. Air entrainment modeling parameters added to the preferences menu of the *MAGMAsoft* user interface.

The total air entrainment by locations can be visualized in the new model. An example of this is shown in Figure 15. Here a jet of liquid flows through the cylindrical inlet into a basin, the fluid flows from the basin through a filter and into a casting. The total air entrainment is the time integrated air entrainment for each computational cell. As shown in Figure 15(b), casting process designers can determine "hot spot" locations where the worst air entrainment occurs. The filling system can be designed to reduce such hot spots. The inclusion generation, filtering and transport model is demonstrated in Figure 16 using this case. The filling temperature field and air entrainment inclusion size distributions at 1 and 9 seconds from the start of filling are shown. Inclusions are generated at locations of air entrainment and are transported by the flow. Note that inclusions are trapped by the filter if they are larger than a critical filtering diameter, in this case 50 microns. Inclusions larger than 50 microns in the casting were generated by air entrainment in the casting. The flow from the filter has a waterfall-like appearance and generates larger amounts of air entrainment and inclusions in the casting. The effects of varying the air entrainment inclusion model parameters is presented in the results section of this paper.

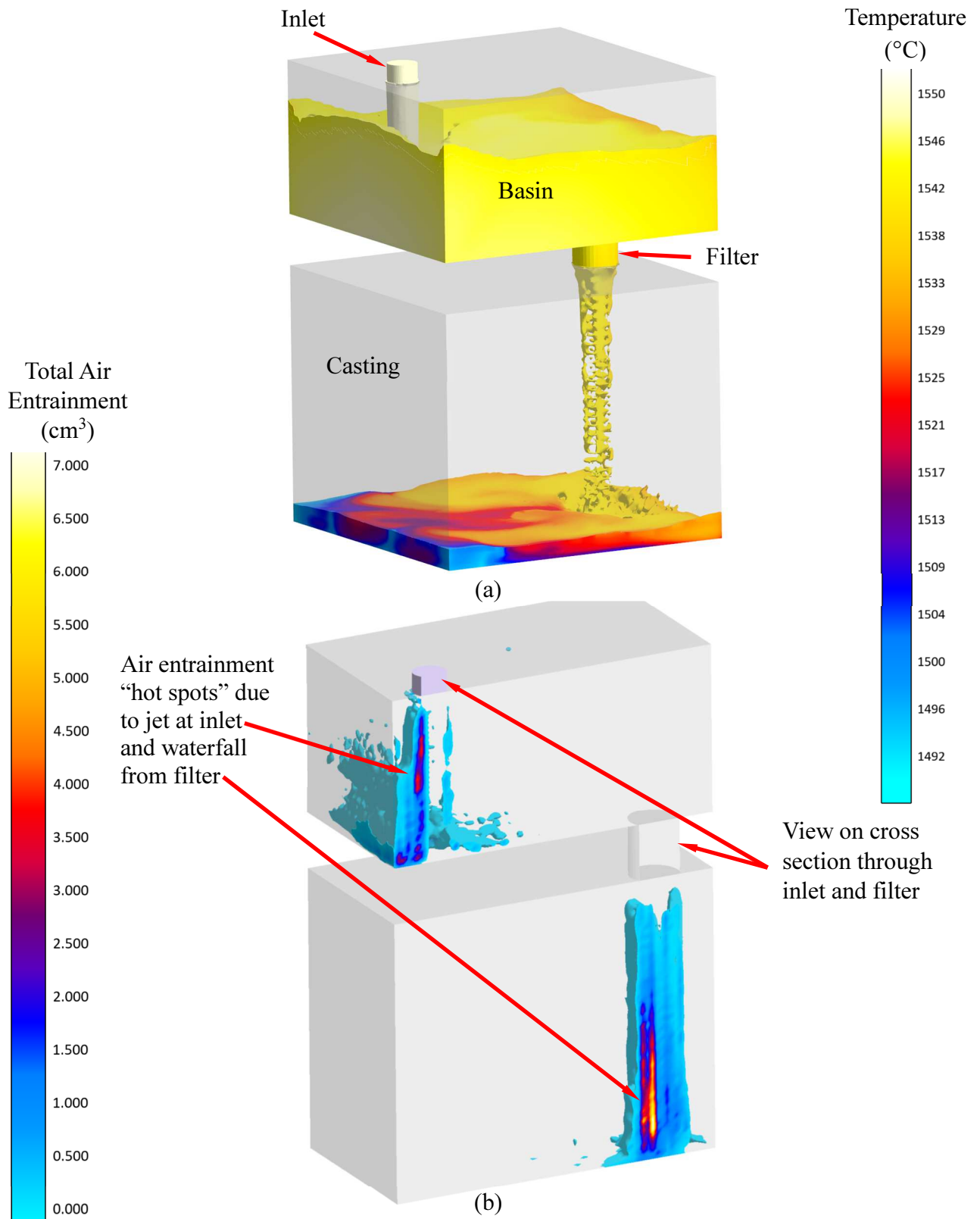


Figure 15. Filling temperature (a) for demonstration of air entrainment inclusion model. Example of air entrainment modeling result in x-ray view (b) the total integrated air entrainment at locations in the casting system during the filling process shown in cross section.

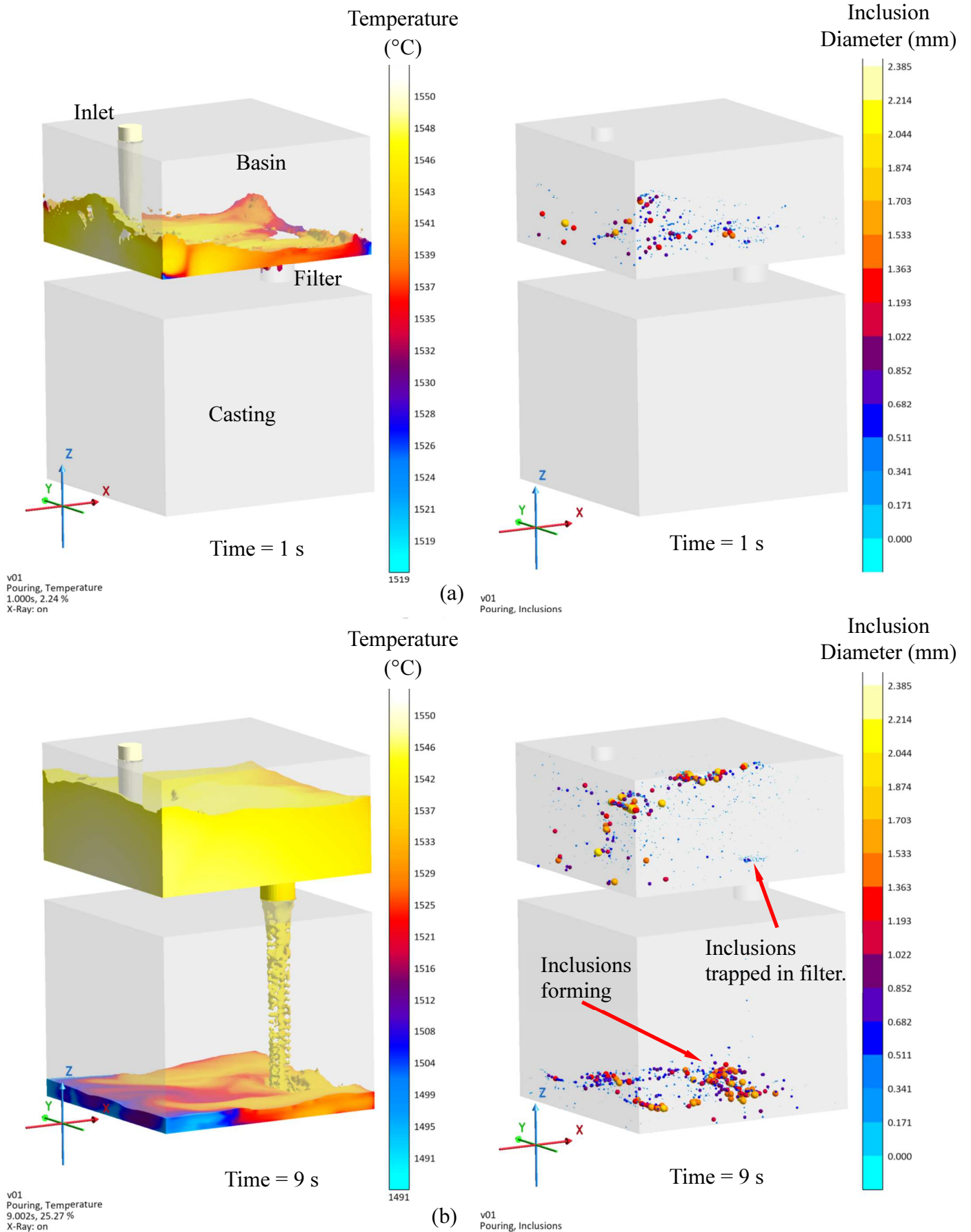


Figure 16. Images of filling temperature and inclusion diameter results at 1 second (a) and 9 seconds (b) after start of filling.

3. Results

3.1 Results of Case Study Measurements

The marked-up surfaces of the solid models were analyzed to determine the inclusion indication sizes, area percentage on the surface and other measured data describing the inclusion distributions. The cope surface images used to analyze the case study castings' measured inclusion results are given in Figures 17 through 23 for castings 4, 5, 6, 7, 8, 9, and 10, respectively. Four castings were poured with a gating system (castings 4, 5, 6, and 7) and three were poured without a gating system by pouring through/into the feeder (castings 8, 9, and 10). Note that the pouring order by casting number is 4, 5, 6, 7, 8, 9, and 10. In Figures 17 through 23 inclusion location areas are indicated in black, and the area percentage of inclusions on the cope surface is given in each figure. The cope surfaces of the casting filled through the feeder clearly have more indications than the bottom filled castings looking at the images.

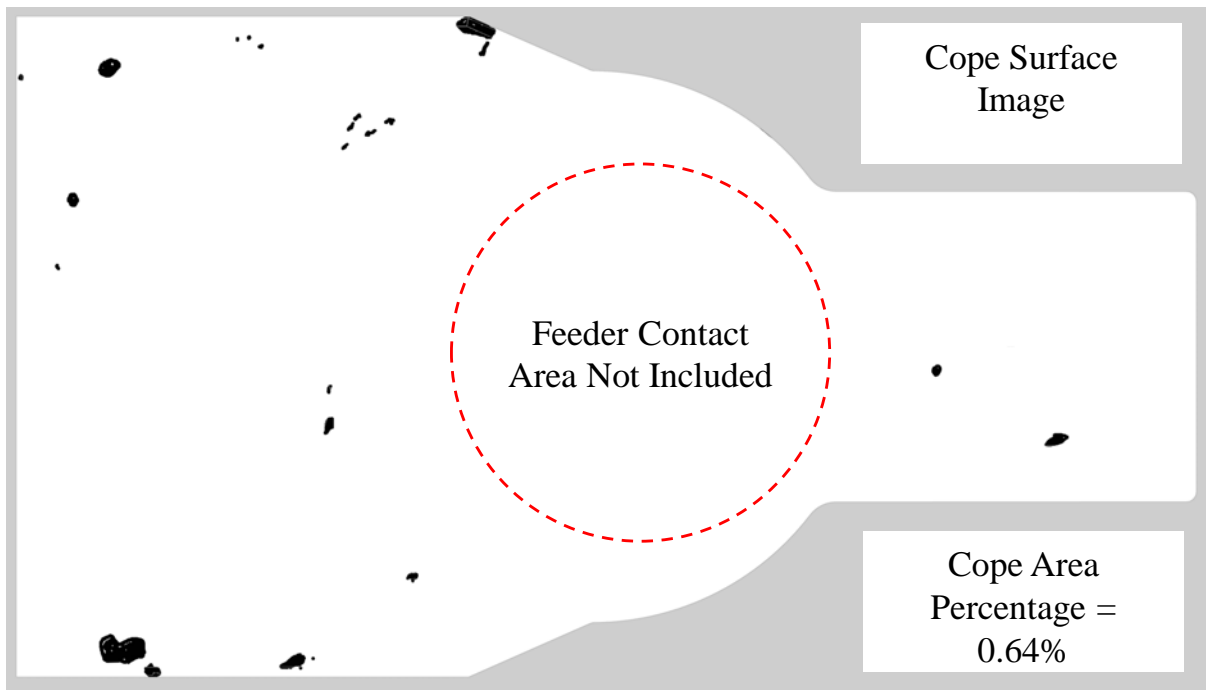


Figure 17. Cope image for analysis and inclusion area percentage calculation for bottom-filled Casting 4.

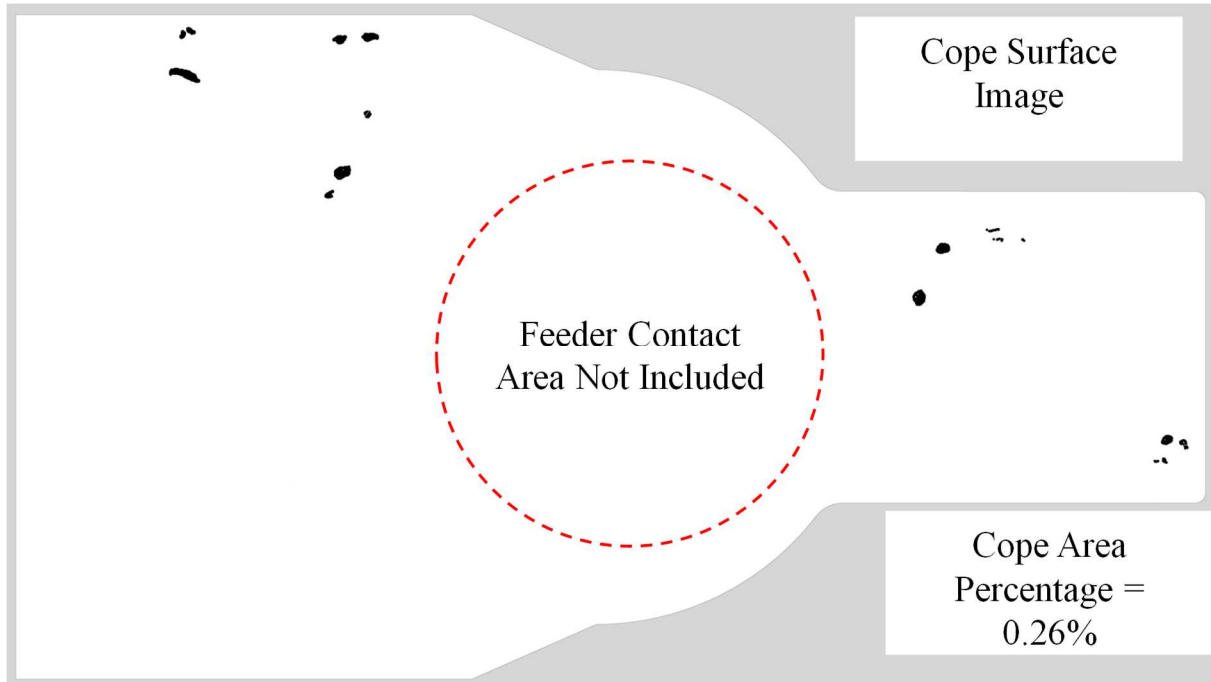


Figure 18. Cope image for analysis and inclusion area percentage calculation for bottom-filled Casting 5.

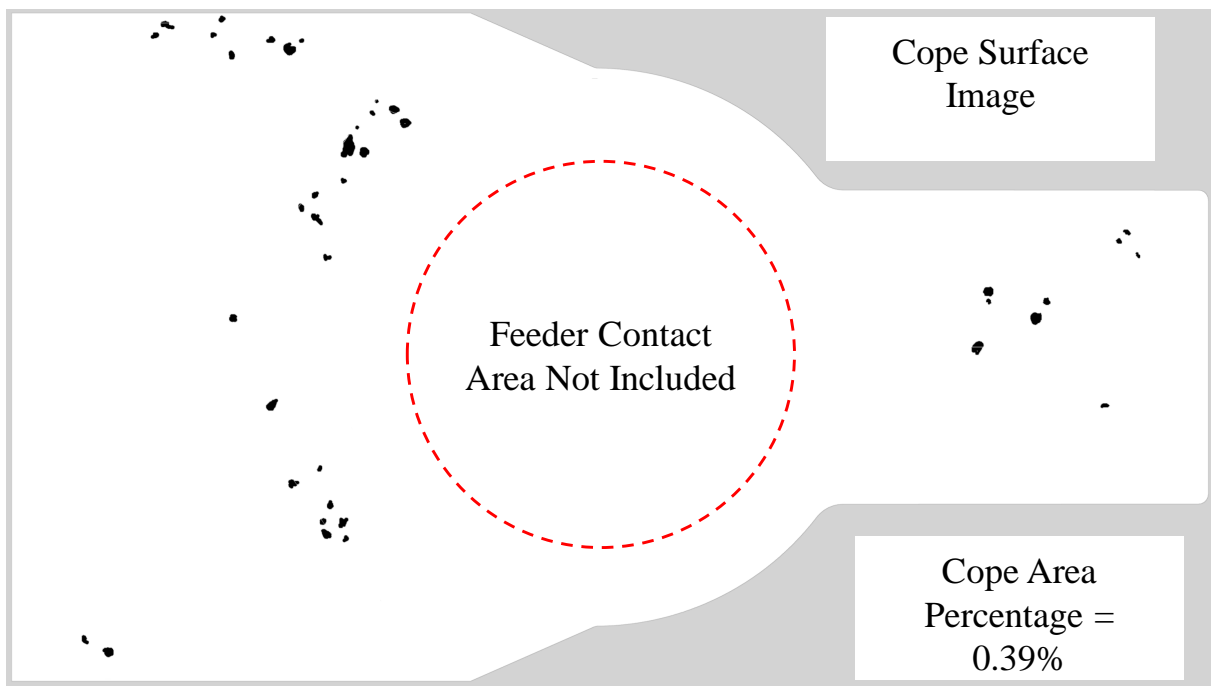


Figure 19. Cope image for analysis and inclusion area percentage calculation for bottom-filled Casting 6.

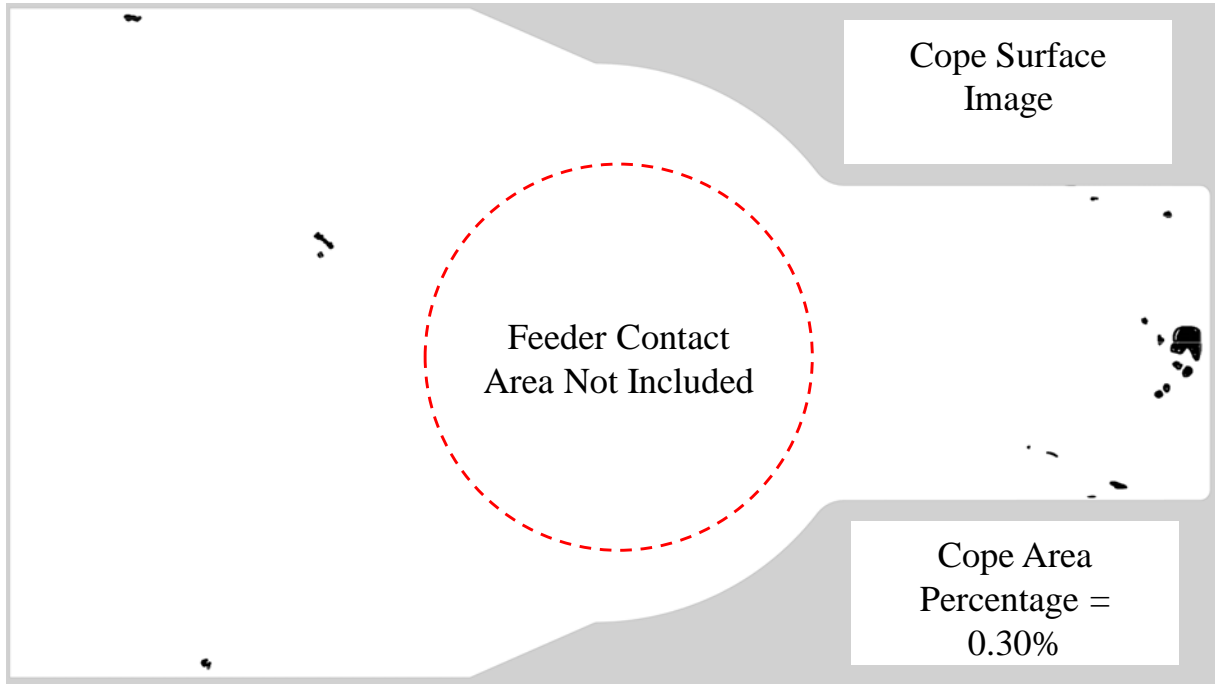


Figure 20. Cope image for analysis and inclusion area percentage calculation for bottom-filled Casting 7.

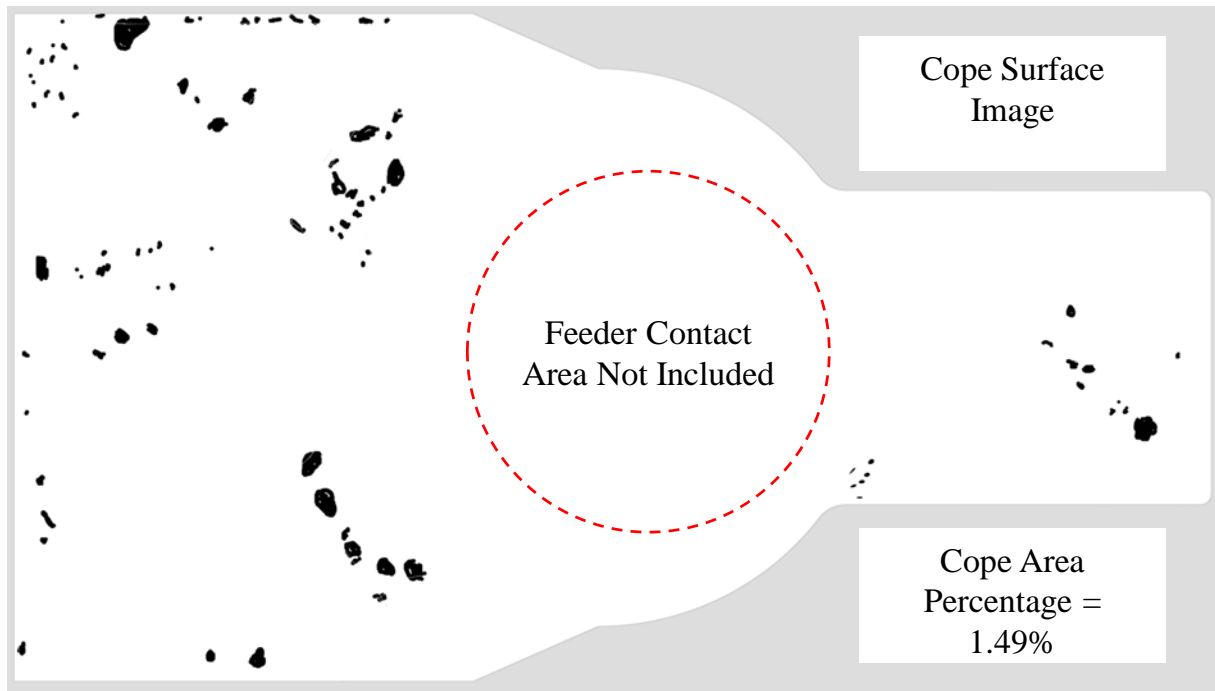


Figure 21. Cope image for analysis and inclusion area percentage calculation for feeder-filled Casting 8.

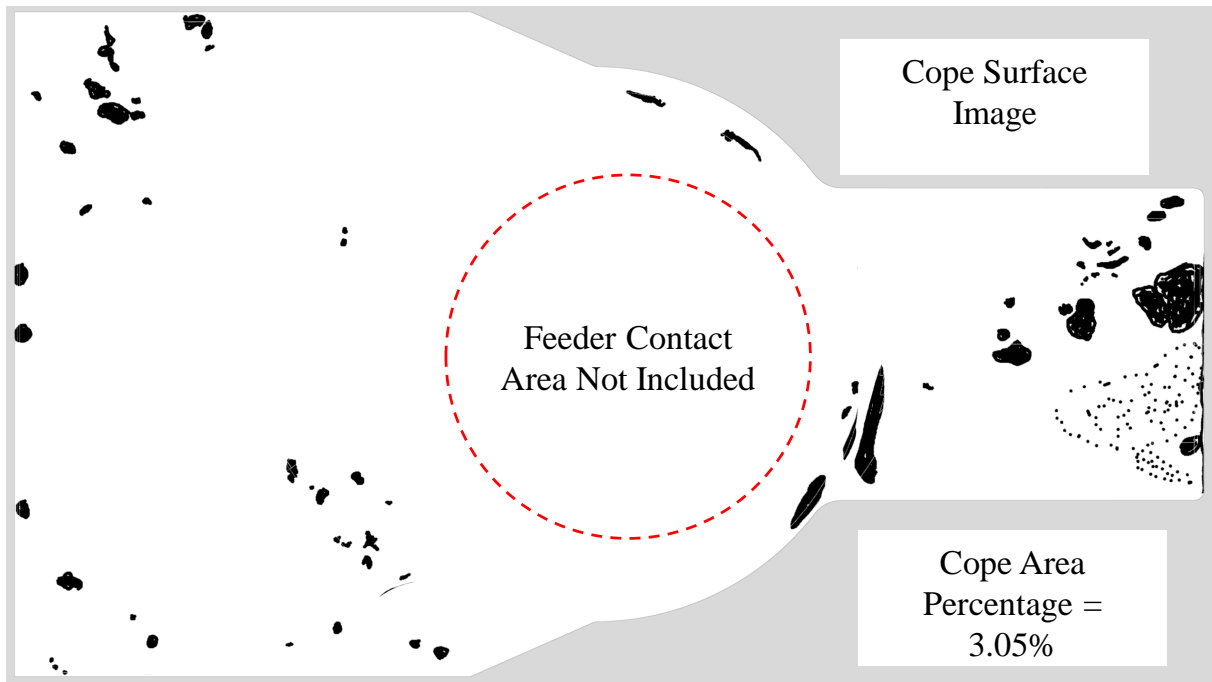


Figure 22. Cope image for analysis and inclusion area percentage calculation for feeder-filled Casting 9.

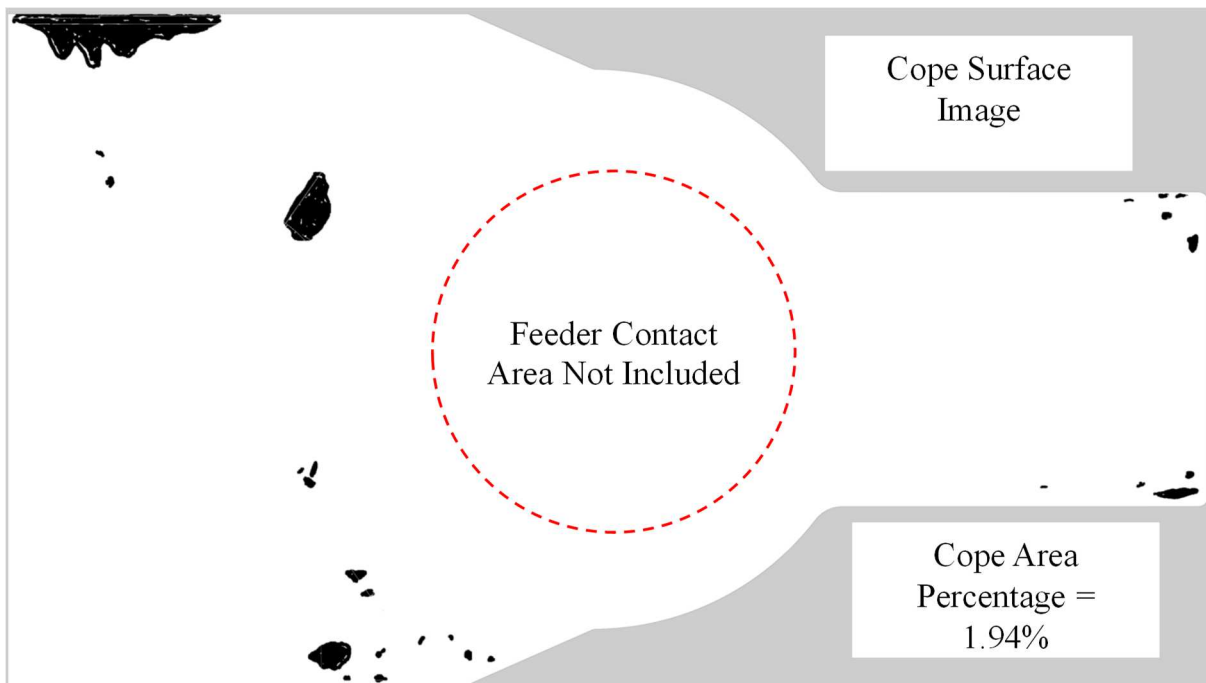
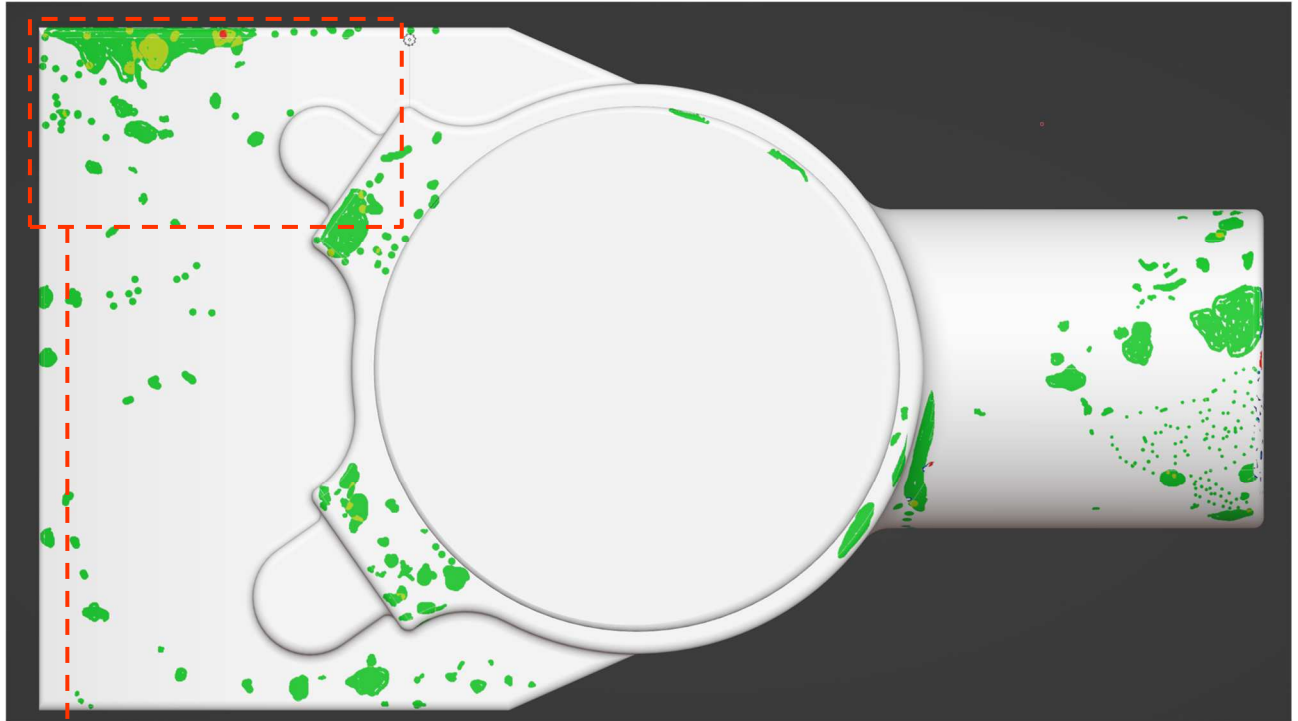


Figure 23. Cope image for analysis and inclusion area percentage calculation for feeder-filled Casting 10.

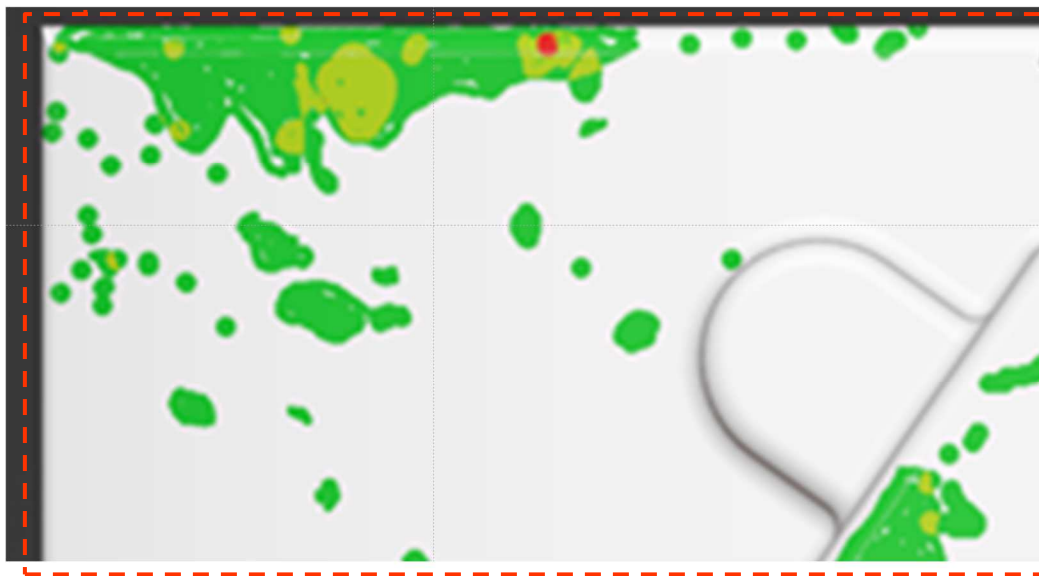
The software *ImageJ* used to analyze the images in Figures 17 to 23 has many capabilities to combine such images using its image math capabilities. These capabilities are used to create probability maps of the inspection results for the two types of gating systems. The four inspection results for the casting cases with bottom gating, and the three inclusion inspection results for the castings filled through the feeder, are combined to determine whether the locations of inclusions are repeatable for the two filling methods. The images are first converted from binary (a 0 or 1, or black and white) to 256 levels by multiplying them by a factor of 256 divided by the number of images to be combined, for the bottom-filled case four images, and for the feeder-filled case three images. The images are next operated on by using image addition where the sums of the levels at each pixel are added together. The value of each pixel is then converted to a color by mapping the pixel values to a color lookup table. The image file for each gating case can be imported into the *Blender* software resulting in a solid model mapped with color levels corresponding to the probability of an inclusion being observed at a given location.

Results of this process are shown in Figure 24 for the three feeder-filled images, and in Figure 25 for the four bottom-filled images. Results in the figures are given for the cope surfaces. In Figure 24 the probability that an inclusion appears at a location in one out of three castings is the color green, two out of three if the color is yellow, and red if all three castings had an indication at that location (100% probability). In Figure 24(a) a region of the casting surface with higher inclusion probability values is outlined and magnified in Figure 24(b). In Figure 24(b) only one relatively small region having an inclusion location probability of 100% is shown. The results for the bottom-filled casting in Figure 25 show even less repeatability, where the probabilities are one out of four to 4 out of four inclusions occurring at a location. In that figure, most indication locations only appear in one out of four castings (blue) with very small regions having two out of four castings with indications at locations on the cope surface. In neither gating case was the locations of indications on the cope surfaces found to be very repeatable.

The results of the inclusion indication area percentage measurements made using image analyses of the cope surfaces shown in Figures 17 to 23 are given in Figure 26(a). The results of the image analyses of the drag surfaces for each casting are shown in Figure 26(b). The area percentages are given for each casting with the castings grouped by whether the gating system was used. For the cope surfaces, Figure 26(a) shows the cases poured with a gating system are consistently cleaner than those poured without a gating system. The cases with gating system have inclusion area percentages ranging from 0.26% to 0.64%, and the castings poured through the feeder have a range from 1.49% to 3.05%. For the drag surfaces, Figure 26(b) shows the cleanest casting poured has a gating system (0.25% area percentage), and the dirtiest casting was poured without a gating system (1.11% area percentage). However, considering all drag surfaces, the area percentages have a similar range and variability regardless of whether the gating system was used. No consistent difference in the area coverage of inclusions on the drag surfaces is observed between the two pouring cases. The results of averaging the measured inclusion area percentages by the castings poured with/without gating system, and cope and drag surfaces, are shown in Figure 27. For the measured cope surfaces, the casting poured with the gating system have an average inclusion area of 0.40% and the cases poured without a gating system have 2.16%. The blue bars in the cope measurements indicate the range of measured data above and below the mean.



(a)



Probability (%)



100%

66%

33%

(b)

Figure 24. Top view (cope surface view) of the combined marked up models in the *Blender* software for riser-filled castings 8, 9, and 10 (a). Magnified region of the casting surface showing that inclusion location areas are indicated by green if one casting out of three has an inclusion there, yellow if two castings have inclusions at that location and red if all three castings have an indication at that location.

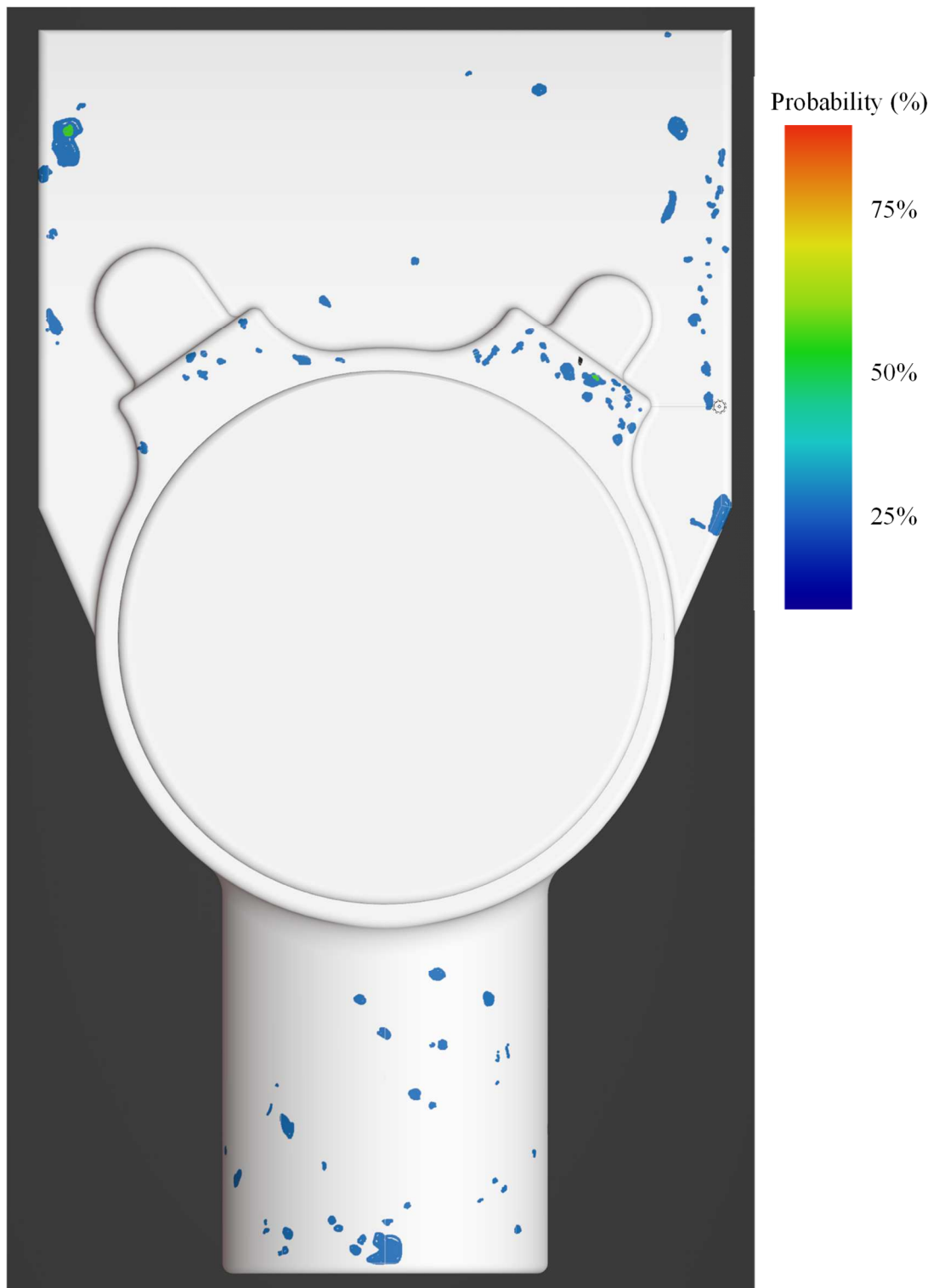


Figure 25. Top view (cope surface view) of the combined marked up models in the *Blender* software for bottom-filled castings 4 through 7. Observed inclusion locations are indicated by blue if one casting out of four has an inclusion there, and green if two castings have inclusions at that location. No more than two out of the four castings had agreeing locations of inclusions.

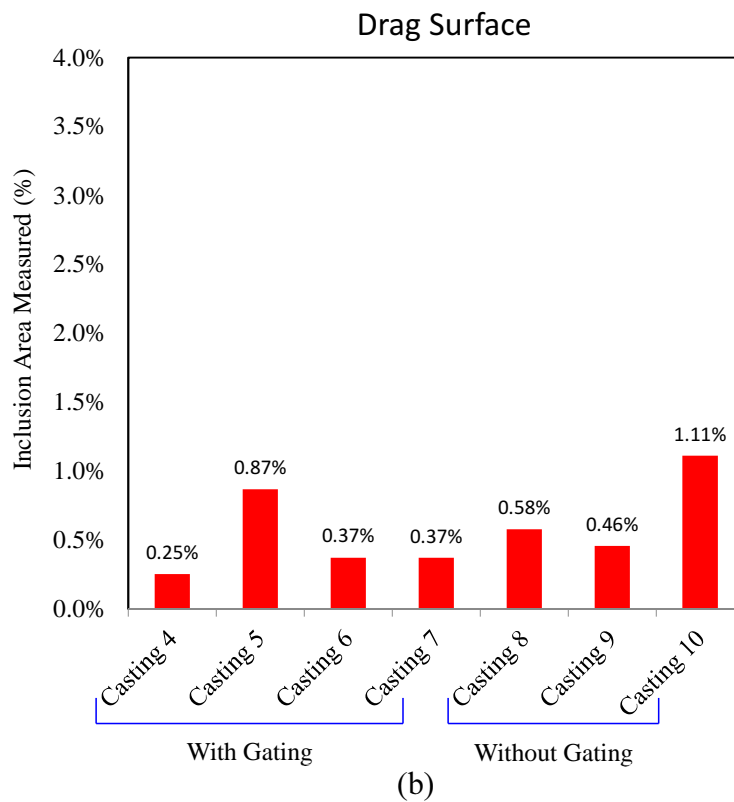
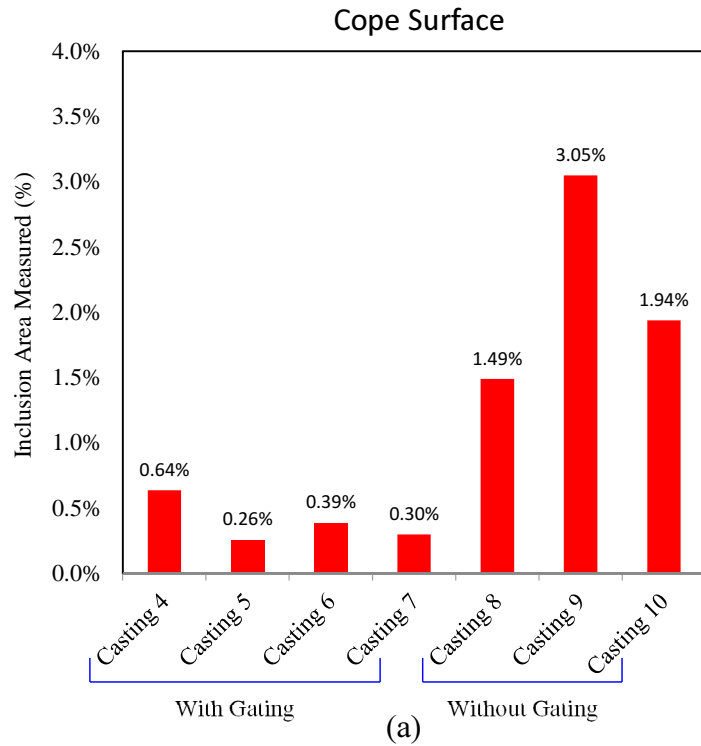


Figure 26. Summary of measured inclusion area percentage by casting for cope surfaces (a) and drag surfaces (b) from the commercial casting case study.

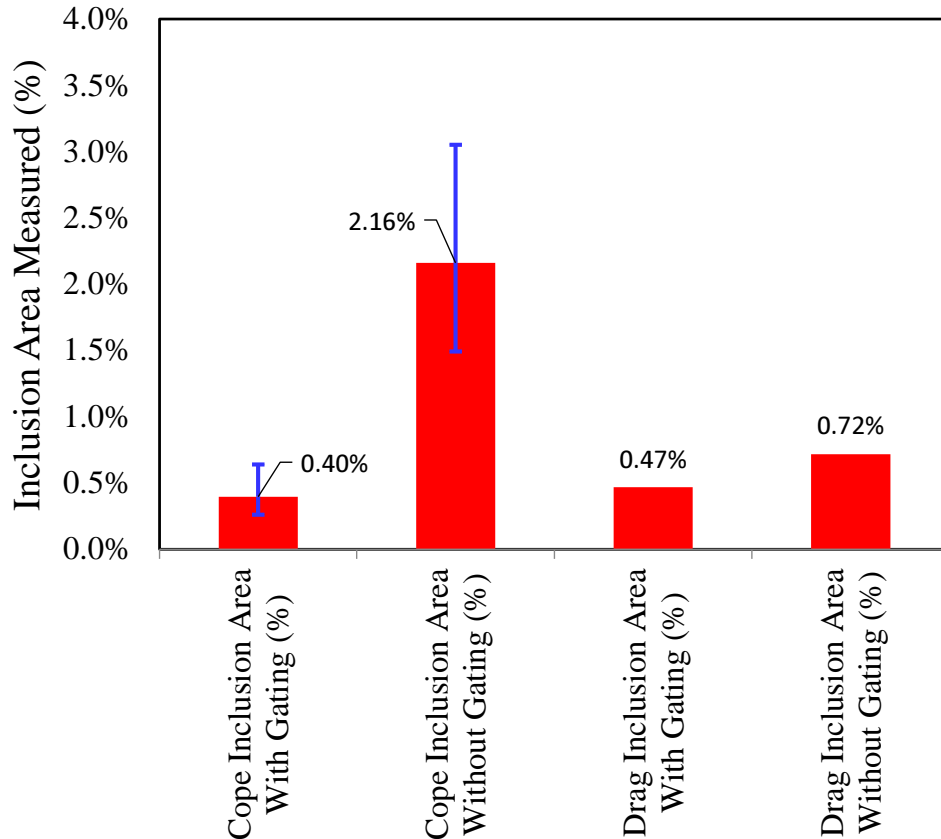


Figure 27. Summary of average measured inclusion area percentage by gating system and cope or drag surfaces from the commercial casting case study.

3.2 Results of Case Study Simulations and Comparisons with Measurements

Simulations were run using the air entrainment inclusion model and its results are compared in this section to the measurements. Simulations were also performed using the dross inclusion model, and results from this model are presented in an Appendix at the end of this paper. Results from the dross model did not agree with the measured results. Since a large bottom poured ladle was used to pour the case study castings described here, it is unlikely that inclusions entering the casting system at the inlet (as assumed in the dross model) were the dominant source of the measured inclusions in the case study. While not applicable in the commercial casting case study presented here, the dross model has been shown to be useful in modeling inclusions for castings poured from a lip poured ladle having a capacity of several hundred pounds [12].

In this section the measured area percentage of inclusions on the cope surface, the inclusion indication count and mean inclusion equivalent diameter are compared to the air entrainment inclusion model results. The analysis of the simulation results is similar to the measurements as described in section 2 of this paper. Images of the inclusion results on the cope surfaces are exported from the casting simulation software and analyzed. The images from the software postprocessor are captured for clipped views of the model "bill" and "tail" sections shown in Figure

28. Since the inclusions are post-processed and displayed in x-ray view, the simulation model results are clipped to exclude inclusions on the drag surface and in the lower part of the casting. By using the clipping process only inclusions on or near the cope surface are evaluated.

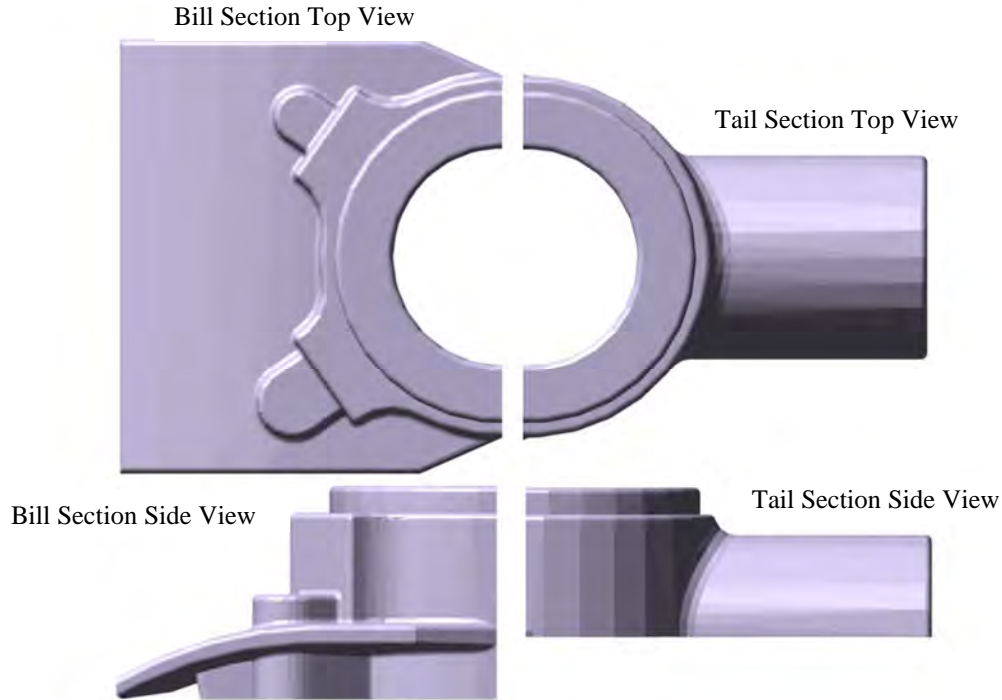


Figure 28. Clipped views of the model "bill" and "tail" sections used to capture images for the inclusion distributions image analysis are shown. The modeling results are clipped to exclude inclusions in the lower part and drag surface of the casting. Only inclusions on or near the cope surface are evaluated.

The inclusion size distribution evolution throughout filling is simulated as shown in Figure 29 for the riser-filled case. The model parameters were varied in a parametric study to determine the model parameters which gave the best agreement with the measured percentage area of inclusions. The best agreement model parameters are; space raster = 2.0 cm, time raster = 1.0 s and mass ratio = 0.05, as given by the text in the figure. The fill times used in the simulations were determined from videos of pouring the castings. These were 12.6 s for the castings poured through the riser and 14.0 s for the bottom-filled castings. Another simulation parameter varied by parametric study to give the best agreement with the measurements was the inlet diameter. A 20 mm inlet diameter was determined to give the best agreement between the measured and simulated inclusion area percentage. This will be discussed later in this section.

For each simulation analyzed, the top view of the final inclusion distribution was exported after scaling it to reflect the predicted inclusion diameter. Then it was magnified by a factor of 1.7 as described in section 2.3 to convert it from a sphere to a disk-shape. The resulting color image, such as that shown in Figure 30(a), was processed in *ImageJ* to a binary image used in the inclusion

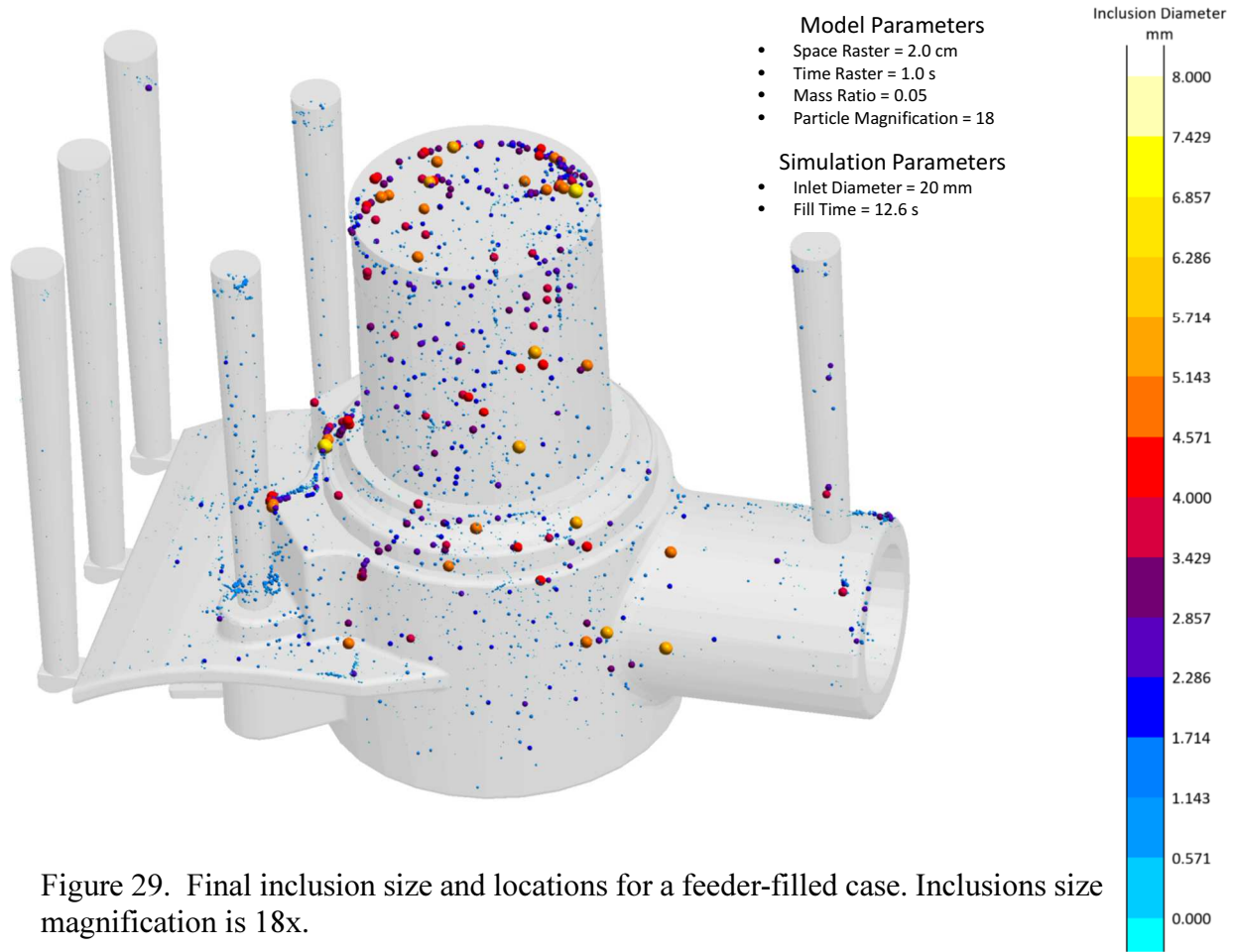
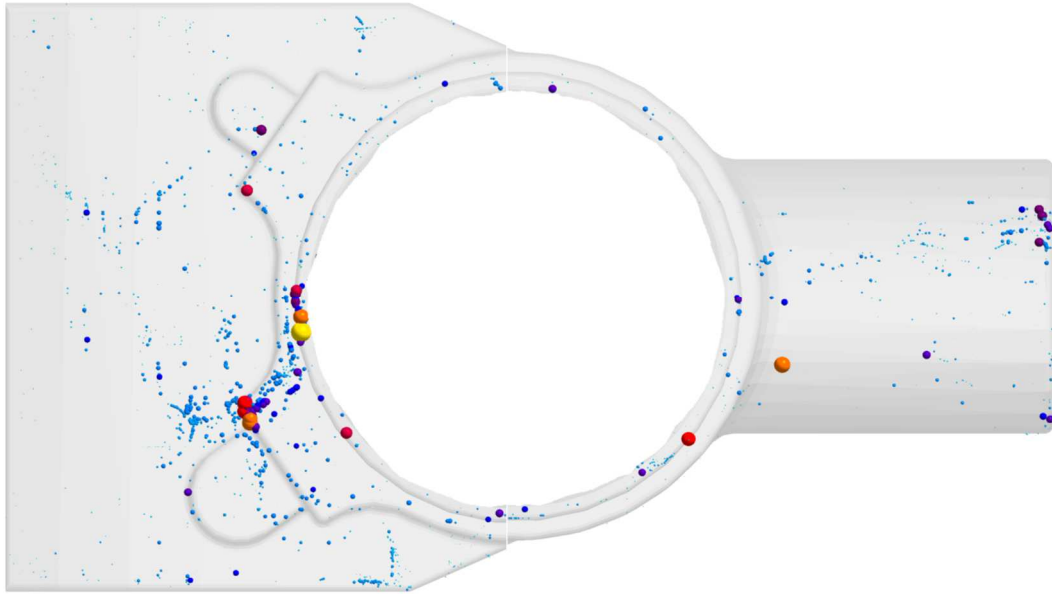


Figure 29. Final inclusion size and locations for a feeder-filled case. Inclusions size magnification is 18x.

image analysis as shown in Figure 30(b). The image analysis results from the particle analysis determined for each simulation case were the same as the measurements: area percentage, inclusion indication count, and mean inclusion equivalent diameter. The parameters used and image analysis results for the case are in the table in Figure 30 and are compared to the measurements. Note that the clustering of the inclusions as seen in Figure 30(b) increases the mean inclusion diameter from the image analysis. The table in Figure 30 shows the measured and simulated inclusion area percentage are 2.16% and 2.15%, respectively. Looking at the inclusion count (number of inclusions) and mean diameter, there are many smaller inclusions in the simulation compared to the measurements. This demonstrates the need to filter out or remove inclusions below a threshold size in the simulations. For the measurements made at the foundry, unmagnified observations were made and there was a size detection limit of approximately 1 mm. It is reasonable to filter out simulated inclusions below this size. A study to determine a reasonable filter size for the analysis of the simulation results is discussed later in this section.



(a)



(b)

	D_{inlet} (mm)	Space Raster (cm)	Time Raster (s)	Mass Ratio	Area %	Count	Mean Diameter (mm)
Simulation Case without Gating	20	2.00	1.00	0.050	2.15%	1109	1.10
Measurement without Gating (%)					2.16%	100	3.74

Figure 30. Images of the cope surface inclusions (a) from the simulation result shown in Figure 29. These are the starting point for the quantitative inclusion analysis in the *ImageJ* software. The images are then converted to binary images as shown in (b) and quantitatively analysed using the software's particle analysis tool. The table below (b) is a comparison of simulation and measurement results.

The castings were produced using a bottom-poured ladle with a 2.5” diameter nozzle. The filling stream will contract as it falls and there was uncertainty in the diameter of the inlet stream to the castings. Considering this the diameter of the inlet stream was varied in a parametric study to see what inlet diameter gives the closest inclusion area percentage on the casting surface. The inlet diameter was varied from 10 to 50 mm in increments of 10 mm. Because the filling time was constant for each gating case, the inlet velocity varies with inlet diameter. This information is given in Table 1 for the cases along with the model parameters used and the simulation and measurement results. The inclusion area percentage results from the inlet diameter parametric study are plotted in Figure 31. The 10 mm inlet diameter produces very large inclusion area percentages on the

Table 1. Summary tables for simulation and measurement results for the inclusion the case study casting. Results are area percentage, inclusion indication count and mean diameter on cope surface for the case with gating (a) and for the case with the casting filled through the feeder (b). Simulation cases in tables have variable inlet diameter with model raster and mass ratio parameters giving the best agreement with measurements.

(a)

Simulation Cases with Gating	D _{inlet} (mm)	Inlet Velocity (m/s)	Space Raster (cm)	Time Raster (s)	Mass Ratio	Area %	Count	Mean Diameter (mm)
v103	10	24.95	2.00	1.00	0.05	8.28%	1049	1.77
v85	20	6.24	2.00	1.00	0.05	0.44%	613	0.56
v105	30	2.77	2.00	1.00	0.05	0.26%	517	0.54
v107	40	1.56	2.00	1.00	0.05	0.28%	558	0.55
v109	50	1.00	2.00	1.00	0.05	0.25%	588	0.54
Measurement with Gating (%)						0.40%	37	3.01

(b)

Simulation Cases without Gating	D _{inlet} (mm)	Inlet Velocity (m/s)	Space Raster (cm)	Time Raster (s)	Mass Ratio	Area %	Count	Mean Diameter (mm)
v104	10	22.27	2.00	1.00	0.05	12.76%	354	3.71
v86	20	5.57	2.00	1.00	0.05	2.15%	1109	1.10
v106	30	2.47	2.00	1.00	0.05	0.37%	735	0.66
v108	40	1.39	2.00	1.00	0.05	0.28%	664	0.60
v110	50	0.89	2.00	1.00	0.05	0.20%	638	0.52
Measurement without Gating (%)						2.16%	100	3.74

casting cope surfaces for both gating cases. Very high air entrainment occurs for that diameter given the high inlet velocity. The 20 mm inlet diameter simulation area percentage results give the best agreement with the measurements for both gating cases, and this diameter was used to generate the simulation results for the case study. Recalling the discussion in the introduction on the effect of turbulence from throttling the ladle flow during filling on air entrainment, throttling was used to control the flow filling these castings according to the foundry personnel observing the pouring. It is believed that using a slightly smaller inlet diameter than the actual stream entering the casting system is introducing the additional turbulence associated with the throttling of the flow. Also, the actual inlet flow stream diameter entering a casting system can be difficult to know with certainty and if the flow is throttled the stream diameter can change with time. Based on this,

selecting the value of 20 mm for the inlet diameter for the cases simulated in the case study is reasonable.

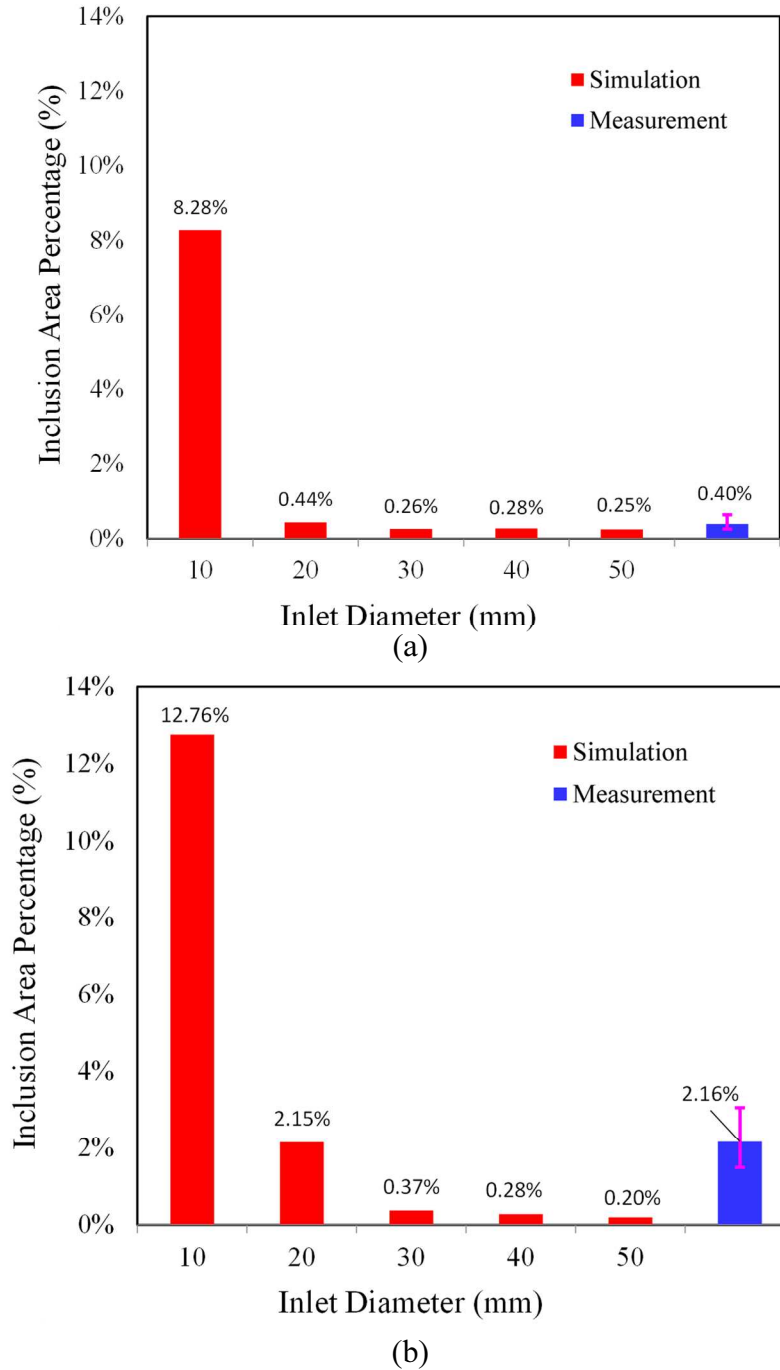


Figure 31. Simulation results for changing inlet diameter compared to measurements for the case study castings with gating (a) and for the casting filled through the feeder (b).

Another parametric study was performed varying the mass ratio in the inclusion model. Decreasing the mass ratio increases the mass of inclusions generated for a given volume of air entrained. With the 20 mm inlet diameter and raster values given in Table 2, the mass ratio was varied. Mass ratios of 0.05, 0.01, 0.005 and 0.001 were used in this parametric study. Based on the inclusion area percentage, the best agreement between measurement and simulation was determined. These results are plotted for both gating cases using the 20 mm inlet diameter in Figure 32. For the 20 mm inlet diameter, the 0.05 mass ratio simulation results have the best agreement compared to the measurements for both gating cases. The results for the bottom-filled gating are shown in Figure 32(a) and for the case poured into the feeder in Figure 32(b). There was concern that a 20 mm inlet diameter might be small compared to the actual inlet stream diameter. Therefore, additionally a mass ratio study was performed using a 30 mm inlet stream diameter. These inclusion area results are given in Figure 33(a) for the bottom-filled and in Figure 33(b) for the riser-filled castings. The data in the plots shows that no single value for the mass ratio produces simulation results that agree with the measurements for both gating cases. A mass ratio of 0.05 produces results agreeing with measurements in Figure 33(a), and a mass ratio between 0.005 and 0.001 produces results agreeing with measurements in Figure 33(b). The best mass ratio parameter to use is shown to be 0.05 along with the 20 mm inlet diameter.

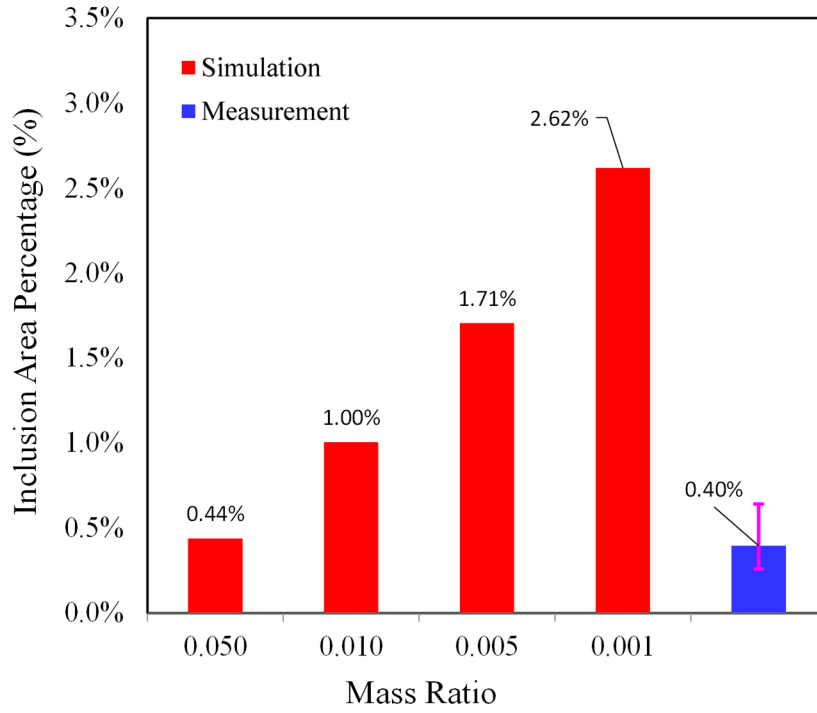
Table 2. Summary tables for simulation and measurement results (inclusion area percentage, count and mean diameter) on cope surface for the inclusion the case study casting. Simulation cases in table have variable mass ratio with other model parameters giving the best agreement with measurements (inlet diameter 20 mm, and space and time raster values are 2 cm and 1 s, respectively). Measured and simulated results for the case with gating (a) and for the casting filled through the feeder (b).

(a)

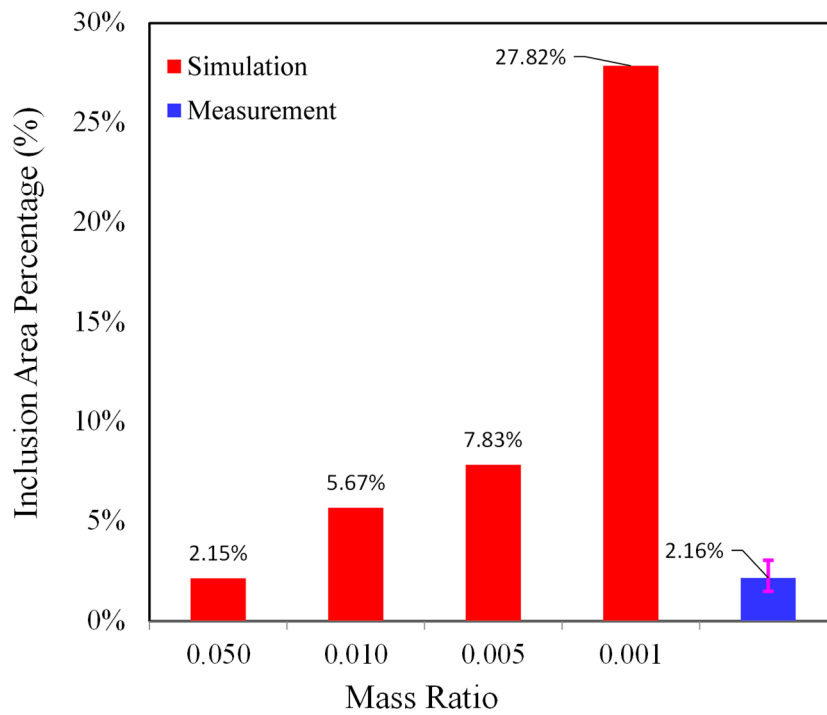
Simulation Cases with Gating	D_{inlet} (mm)	Space Raster (cm)	Time Raster (s)	Mass Ratio	Area %	Count	Mean Diameter (mm)
v85	20	2.00	1.00	0.050	0.44%	613	0.56
v113	20	2.00	1.00	0.010	1.00%	807	0.79
v115	20	2.00	1.00	0.005	1.71%	853	0.89
v117	20	2.00	1.00	0.001	2.62%	917	1.18
Measurement with Gating (%)					0.40%	37	3.01

(b)

Simulation Cases without Gating	D_{inlet} (mm)	Space Raster (cm)	Time Raster (s)	Mass Ratio	Area %	Count	Mean Diameter (mm)
v86	20	2.00	1.00	0.050	2.15%	1109	1.10
v114	20	2.00	1.00	0.010	5.67%	881	1.70
v116	20	2.00	1.00	0.005	7.83%	781	1.91
v118	20	2.00	1.00	0.001	27.82%	538	3.69
Measurement without Gating (%)					2.16%	100	3.74

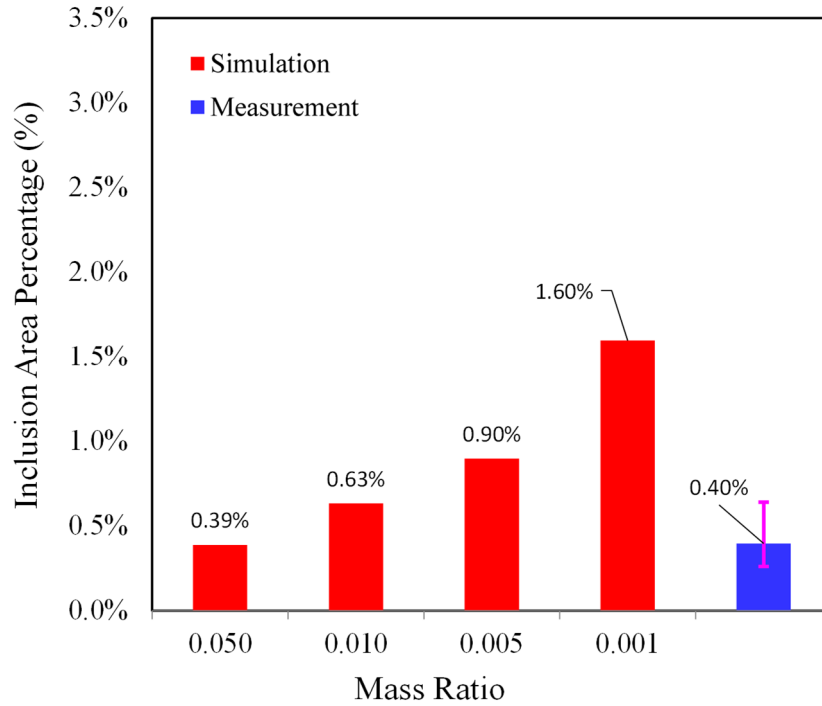


(a)

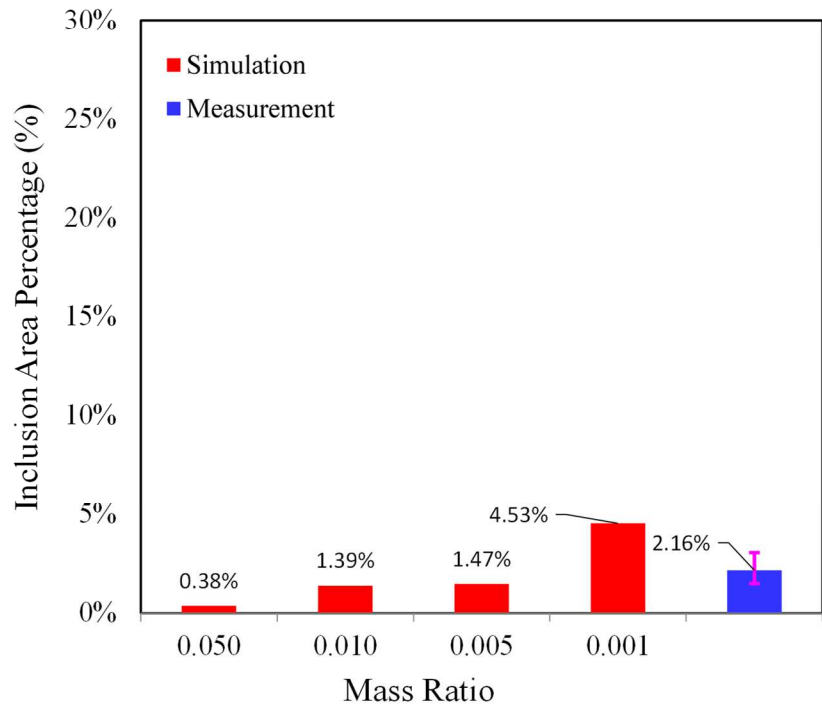


(b)

Figure 32. Simulation results for changing mass ratio with inlet diameter of 20 mm and space and time raster values are 2 cm and 1 s, respectively, are compared to measurements for the case study castings with gating (a) and for the casting filled through the feeder (b).



(a)

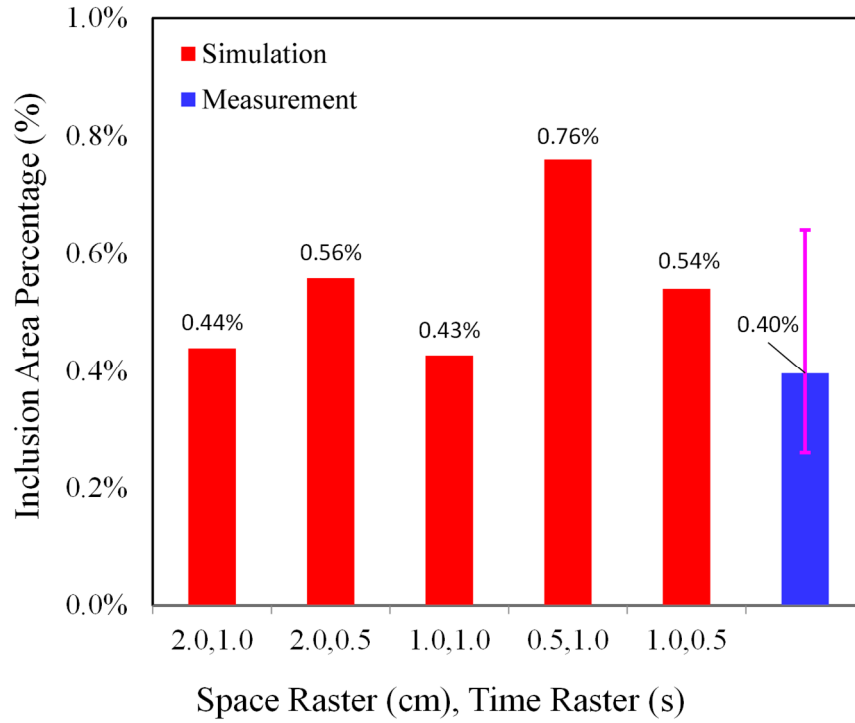


(b)

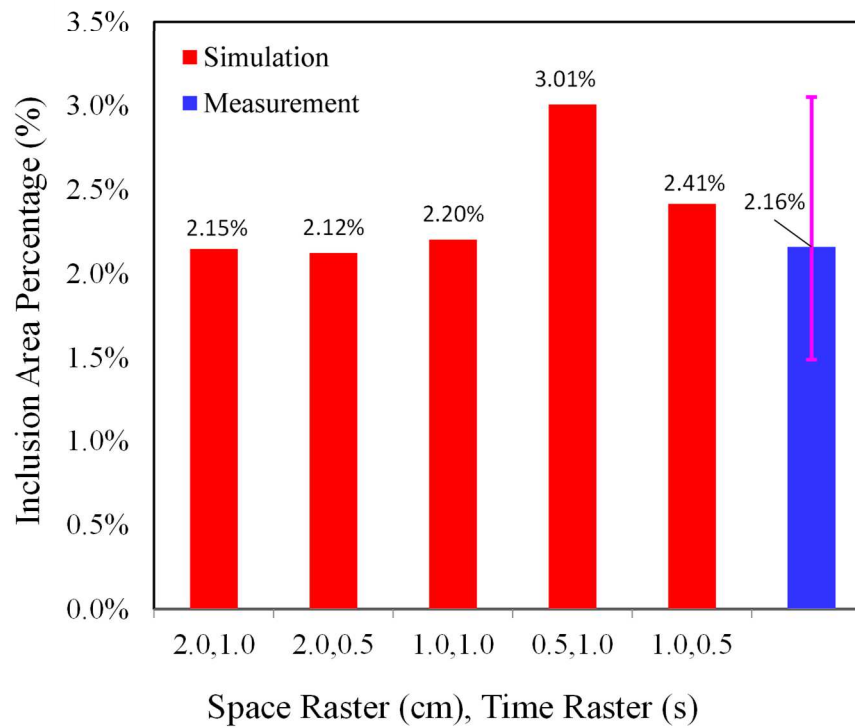
Figure 33. Simulation results for changing mass ratio with inlet diameter of 30 mm and space and time rasters are 2 cm and 1 s, respectively, are compared to measurements for the case study castings with gating (a) and for the casting filled through the feeder (b).

A parametric study was performed varying the space and time raster parameters in the inclusion model. During development of the air entrainment inclusion model, it was found that values for the space raster of 1.0 cm and the time raster of 0.5 seconds produced reasonable predictions compared to inclusion tracking experiments [13]. However, a parametric study using industrial measurements was not performed until this work. The parametric study varied the space raster with values of 2.0, 1.0 and 0.5 cm, and the time raster with values of 1.0 and 0.5 s. The combinations of the two raster parameters used in the study (given in the format “space raster, time raster”) were “2.0,1.0”, “2.0,0.5”, “1.0,1.0”, “0.5,1.0”, and “1.0,0.5”. The inclusion area results for the parametric study are given in Figure 34(a) for the bottom-filled and in Figure 34(b) for the riser-filled castings. The results for the default values “1.0,0.5” give reasonable results within the range of the casting measurements for both gating cases. Considering the measurement averages given in the figures, the model raster values “2.0,1.0” give the best agreement with measurements, and values of “1.0,1.0” also give good results. Based on the parametric study results, raster values of “2.0,1.0” are recommended. However, it is good to observe that the sensitivity of the model results is not great for a range of space raster values from 2.0 to 1.0 cm and time raster values from 1.0 to 0.5 seconds.

As mentioned previously, it is reasonable to filter out small inclusions in the analysis of the simulation results which could not have been detected in the measurements. During the inspection of the casting surfaces, it was difficult to identify inclusions smaller than approximately 1 mm. A study was performed filtering out inclusions smaller than 0.5, 1, 1.5, 2 and 3 mm with the goal of having the simulated mean inclusion size agree more closely with the measurements. The filtered size results were also compared to the unfiltered results (filter size of 0). Another objective of the study was to demonstrate that the filter size has only a small effect on the inclusion area percentage resulting from the simulations. The results of the filter study are given in Table 3. The simulation inclusion mean diameter increases with increasing filter size. Over the range of filter sizes the simulations agree with the measured mean inclusion size. For example, the simulation mean inclusion diameter for the case with gating agrees with the measured mean inclusion size (3.01 mm) when using a filter size between 1.0 and 1.5 mm. To visualize the effect of filter size on the inclusion area percentage and mean inclusion diameter, those simulation results are plotted in Figure 35(a) and Figure 35(b), respectively. The measurements are plotted in Figure 35 as horizontal dashed lines with red and blue denoting the gating used. These figures show very little difference in sensitivity of the two gating cases to filtering for the mean inclusion diameter in Figure 35(b). While for the inclusion area percentage in Figure 35(a), the case without gating (poured into the feeder) is very sensitive to filtering, and the case with gating has very little sensitivity to filtering. The selection of the best filter size is determined from the lowest overall difference between measured and simulated inclusion area percentage and mean diameter for both gating cases. Examining the plots in Figure 35, the smallest differences for both simulated gating cases compared to measurements are filter sizes of 1.0 mm (17.5% difference) and 1.5 mm (15.6% difference). It is good that filtering in this range does not have a big effect on the results, and that either filtering level works well. Note that a filter size of 1.5 mm has the lowest difference compared to measurements for mean diameter, and a filter size of 0.5 mm has the lowest difference compared to measurements of inclusion area percentage. A filter size of 1.5 mm has the lowest difference for both area percentage and diameter. This size is recommended.



(a)



(b)

Figure 34. Simulation results for changing space and time raster values with constant mass ratio of 0.05 and 20 mm inlet diameter are compared to measurements for the case study castings with gating (a) and for the casting filled through the feeder (b).

Table 3. Summary tables for simulation and measurement results. Simulation cases in table have variable filter size with other model parameters giving the best agreement with measurements. Measured and simulated results for the case with gating (a) and case without gating (b).

(a)

Simulation Cases with Gating	D_{inlet} (mm)	Filter Size (mm)	Space Raster (cm)	Time Raster (s)	Mass Ratio	Area %	Count	Mean Diameter (mm)
v85	20	0.00	2.0	1.0	0.05	0.44%	613	0.56
v85	20	0.50	2.0	1.0	0.05	0.39%	83	2.09
v85	20	1.00	2.0	1.0	0.05	0.38%	61	2.52
v85	20	1.50	2.0	1.0	0.05	0.36%	38	3.33
v85	20	2.00	2.0	1.0	0.05	0.34%	29	3.84
v85	20	3.00	2.0	1.0	0.05	0.30%	19	4.54
Measurement with Gating (%)						0.40%	37	3.01

(b)

Simulation Cases without Gating	D_{inlet} (mm)	Filter Size (mm)	Space Raster (cm)	Time Raster (s)	Mass Ratio	Area %	Count	Mean Diameter (mm)
v86	20	0.00	2.0	1.0	0.05	2.15%	1109	1.10
v86	20	0.50	2.0	1.0	0.05	2.12%	738	1.49
v86	20	1.00	2.0	1.0	0.05	1.98%	391	2.16
v86	20	1.50	2.0	1.0	0.05	1.83%	244	2.73
v86	20	2.00	2.0	1.0	0.05	1.65%	157	3.28
v86	20	3.00	2.0	1.0	0.05	1.29%	63	4.71
Measurement without Gating (%)						2.16%	100	3.74

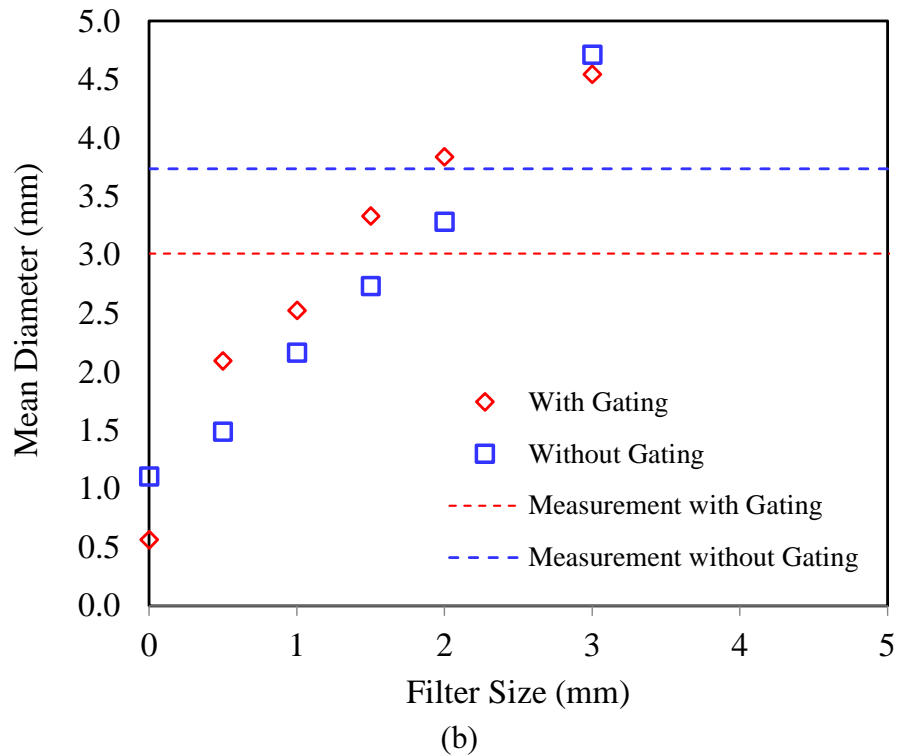
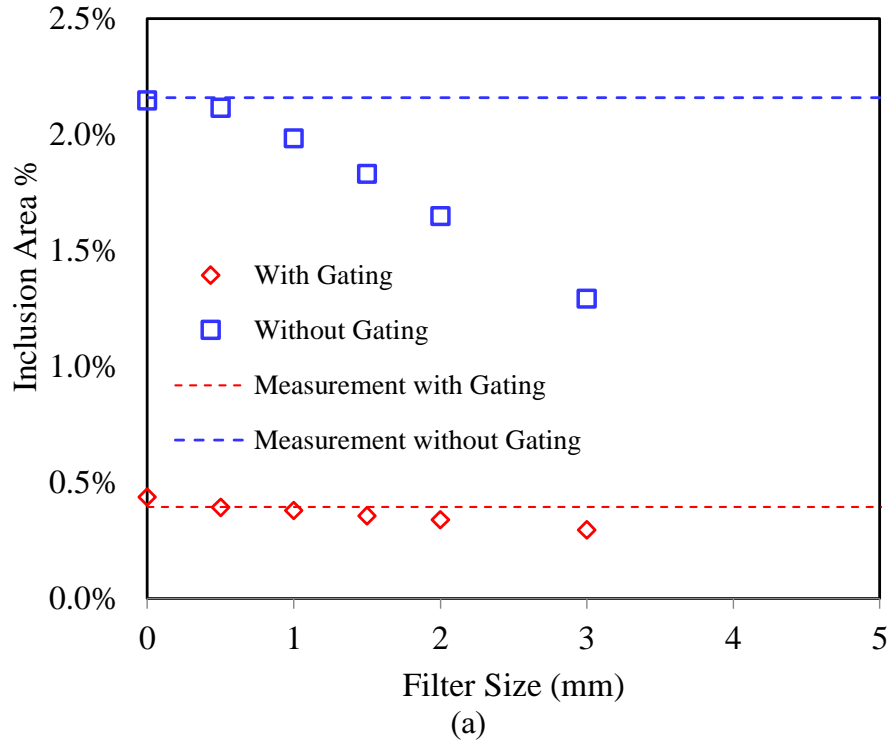


Figure 35. Results of inclusion size filtering applied in the analysis of the simulation results showing effect of filter size on inclusion area percentage on the casting surface (a) and inclusion mean diameter (b). Symbols are simulation results where red denotes the bottom-filled gating case and blue denotes the feeder-filled case.

4. Conclusions

Measurements and simulations were performed for a production casting case study investigating oxide inclusions. The castings were poured at a Steel Founders' Society of America (SFSA) member foundry using a 20-ton bottom-pour ladle with a nozzle having a 2.5" diameter opening. The casting chosen for the case study is specified as part of a qualification process for foundries to produce castings for the United States Navy. In the case study, four castings were poured using a bottom-filled gating system, and three were poured directly into a feeder without a gating system. The main objective of the case study was to compare the inclusion inspection measurement results and simulation predictions for the two casting rigging cases.

The results of the inclusion measurements made on the castings' cope surfaces were analyzed to determine if there were differences in the area coverage of inclusions on the casting surfaces. The castings poured with a bottom-filled gating system were consistently cleaner than those poured without a gating system, having inclusion area percentages ranging from 0.26% to 0.64%. Castings poured through the feeder had a range of inclusion area percentage from 1.49% to 3.05%. For the drag surfaces, the cleanest casting poured has a gating system (0.25% area percentage), and the dirtiest casting was poured without a gating system (1.11% area percentage). Overall, for the drag surfaces, the area percentages had a similar range and variability regardless of whether the gating system was used. On average, the bottom-filled castings had 0.4% inclusion area coverage on the casting cope surfaces and the feeder-filled castings had 2.2% inclusion area percentage. Observed inclusion locations on the surfaces were not repeatable for either gating system. Only at one small location for the feeder-filled castings did all three castings have a repeated inclusion appearing.

Simulations were performed using a model where inclusions form from the local air entrainment rate calculated from disturbances at the free surface of the filling flow. This air entrainment inclusion model predicts the formation, transport, and final locations of oxide inclusions in the castings system generated by air entrainment. Measured and simulated inclusion area, count, and size were compared to determine the modeling parameters giving the best agreement with the measurements. In these parametric studies, recommended model parameters giving the best agreement with the measured percentage area of inclusions were determined, and are; space raster = 2.0 cm, time raster = 1.0 s and mass ratio = 0.05.

A study considering the range of diameters of the inlet stream from 10 to 50 mm gave an inlet diameter of 20 mm as producing inclusion area percentages on the cope surfaces closest to the measurements for both gating systems. An inlet stream of 20 mm diameter is smaller than the diameter of the filling stream falling from a ladle having a 2.5" diameter nozzle (63.5 mm) for the range of falling heights estimated from videos of the castings being poured. It remains an open question why simulating a 20 mm inlet stream gave the best agreement to measurements. However, since the flow of metal from the ladle required throttling to control the filling of these castings, it must be that the turbulence generated by throttling is better modeled by using the smaller inlet diameter. This smaller inlet diameter results in higher filling jet velocities and more air entrainment and inclusion formation during filling giving agreement with the measurements.

It was demonstrated that filtering the size of inclusions considered in the analysis of the simulations results resulted in better agreement with the measured mean inclusion diameters. The smallest differences for both gating cases comparing measured and simulated average inclusion diameters are 17.5% difference for filtering out inclusions smaller than 1.0 mm and 15.6% difference filtering out inclusions smaller than 1.5 mm. Filtering in this range did not have a big effect on the results.

Considering all the lessons learned in this case study, using the best model parameters, the 20 mm inlet diameter, and a 1.5 mm filter on the model results, the predicted and measured inclusion area fractions on the cope surfaces for the cases with bottom-filled gating are 0.36% and 0.4%, respectively. For the castings without gating, poured into the feeder, the predicted and measured inclusion area fractions on the cope surfaces are 1.83% and 2.16%, respectively. The percentage differences between the predictions and measurements for these cases are 9.5% with gating and 15.2% for the feeder-filled case.

This case study has produced encouraging results demonstrating the accuracy of a model predicting the amount of inclusions forming during the filling process. Measured and simulation results were analyzed for the cope surfaces and agree well. So, the ability to predict of the final inclusions' locations on the cope surface generally has been demonstrated. The measurements did not reveal any reproducibility of inclusion locations at specific locations on the casting surfaces. The ability to predict inclusions at specific locations will require many more experiments for a given filling cases and geometry, and more careful control of the filling process. In future work, the prediction of the amount of inclusions appearing at specific final locations is worth pursuing. Even if not that, the prediction of the final inclusion locations should be developed where inclusions captured by the gating system, ending up in feeders and controlled through well designed filling flow to predetermined final locations in the casting system. The simulation capability to predict the transport of inclusions to final locations requiring no removal or repair will be a very valuable tool in producing cleaner steel castings and more efficient casting processes.

Acknowledgements

This research is sponsored by the DLA-Troop Support, Philadelphia, PA and the Defense Logistics Agency Information Operations, J68, Research & Development, Ft. Belvoir, VA.

References

- [1] J.M. Svoboda, R.W. Monroe, C.E. Bates and J. Griffin, "Appearance and Composition of Oxide Macroinclusions in Steel Castings," AFS Transactions, Vol. 95, pp. 187-202, 1987.
- [2] J.A Griffin and C.E. Bates, "Ladle Treating, Pouring and Gating for the Production of Clean Steel Castings," Steel Founders' Society of America Research Report No. 104, 1991.
- [3] H. Chanson: Hydraulics of Dams and River Structures, 2004, London, England, pp. 3-15.
- [4] H. Chanson: Journal of Hydraulic Research, 2013, vol. 51(3), pp. 223-243.
- [5] A.J. Melendez, K.D. Carlson and C. Beckermann, "Modelling of Reoxidation Inclusion Formation in Steel Casting", Int. J. Cast Metals Research, 2009, Vol. 32, pp. 624-638.

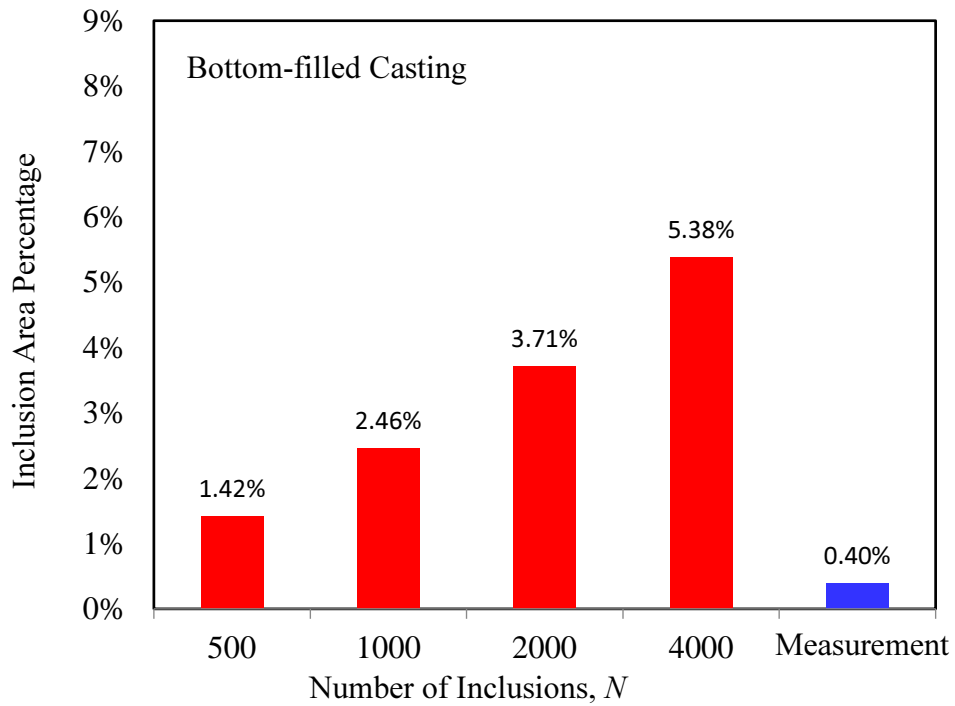
- [6] Majidi, S.H., and Beckermann, C., "Modelling of Air Entrainment During Pouring of Metal Castings," *Int. J. Cast Metals Research*, Vol. 30, 2017, pp. 301-315.
- [7] Melendez A., Carlson K., and Beckermann C. 2010 *Int. J. Cast Metals Res.* 23 278-88.
- [8] MAGMAsoft, MAGMA GmbH, Kackerstrasse 11, 52072 Aachen, Germany.
- [9] D. A. Ervine, E. McKeogh, and E. M. Elsayy: *Proceedings of the Institution of Civil Engineers*, 1980, vol. 69(2), pp. 425-45.
- [10] D. A. Ervine and A. A. Ahmed: Paper E1, *Int. Conf. Hydraulic Modeling of Civil Engineering Structures*, Coventry, England, 1982.
- [11] Majidi S, Beckermann C, Fainberg, J, Schaefer W, and Bodenbun M 2018 *Mat. Sci. Forum* 925 419-26.
- [12] Donahue, R., Hardin, R., and Beckermann, C., "Modeling of Oxide Inclusions in Steel Casting," *IOP Conf. Series: Materials Science and Engineering*, Vol. 1281, 2023, 012035 (8 pages).
- [13] Donahue, R., Hardin, R., and Beckermann, C., "Effects of Gating System and Casting Geometry on Oxide Inclusions in Steel Castings," in *Proceedings of the 75th SFSA Technical and Operating Conference*, Paper No. 4.11, Steel Founders' Society of America, Chicago, IL, 2021.

Appendix

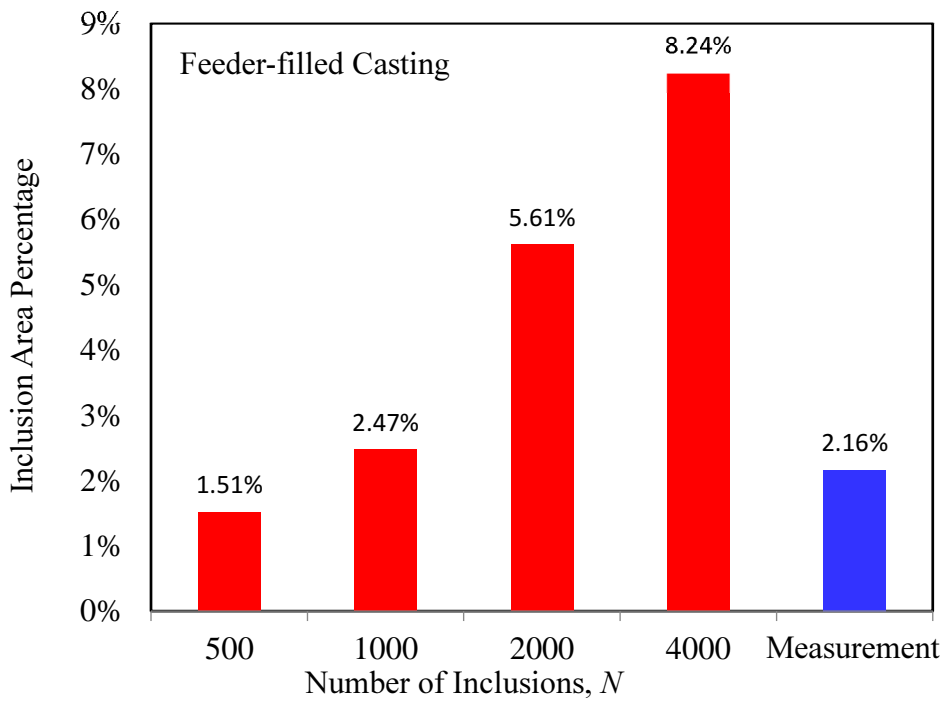
Results of the Case Study Using Dross Inclusion Model

The appendix to the case study describes the simulations run using the dross inclusion model, its results, and comparisons to the measurements. This modeling approach assumes that a distribution of inclusions only enters the casting system at its inlet during the filling. The distribution of inclusions is defined by the number N and size distribution of inclusions, prescribed about a mean diameter D . The size ranges from 50% to 150% about the mean. The inclusion motion model, and method of generating the simulation results are the same used in the air entrainment inclusion model.

As shown in Table 1, the average measured inclusion indication diameter was about 3 mm for the bottom-filled castings and 3.7 mm for the feeder-filled castings. Therefore, it is reasonable to test the dross inclusion model with a distribution of inclusions entering the inlet having a mean diameter D of 3.7 mm to simulate the feeder-filled castings. This was done, and a range of the number of inclusions entering the inlet N during filling from 500 to 4000 was used to study the effect of the parameter N . The inclusion area percentage results for this study are shown in Figure A1(a) for the bottom-filled castings and Figure A1(b) for the feeder-filled castings. For the bottom-filled castings all inclusion area percentage results are much greater than the measurement. In order to simulate agreement with the measurements the parameter N would need to be much smaller than 500 for the case in Figure A1(a). For the feeder-filled casting in Figure A1(b), the study shows a parameter N value between 500 and 1000 would achieve good agreement with the measurements.



(a)



(b)

Figure A1. Inclusion area percentage results on the cope surface for measurements (blue bars), and simulations (red bars) with inclusion number at the inlet (N) ranging 500 to 4000 and mean diameter of inclusions entering the inlet (D) of 3.7 mm. Results are for case study casting with bottom-filled gating (a) and the case for the casting filled through the feeder (b).

However, since the same parameters need to be used for both gating configurations, the dross model using a 3.7 mm mean diameter cannot be used to accurately model the case study castings.

Simulations were run iteratively using the dross model and its results analyzed to try to improve the agreement between the measured and simulated inclusion data using various values on N and D . Figures A2, and A3 give some final comparisons of the area percentage, and mean inclusion equivalent diameter for the simulation cases and the measurements for the castings with and without gating systems. In these figures the inclusion number parameter at the inlet (N) is ranging 1200 to 2000 and mean diameter of inclusions parameter entering the inlet (D) is ranging from 1.5 to 2.1 mm. In Figure A2(a) for the casting with bottom-filled gating, the area percentage in all simulations (red bars) are high relative to the measurements (blue bars). In Figure A2(b) for the casting filled into the feeder without gating, the area percentage in all simulations (red bars) are low relative to the measurements (blue bars). This demonstrates the difficulty in achieving agreement with the measured inclusion area percentage for both gating cases using the dross model with a given set of parameters N and D . Many additional simulation cases were run, but the lowest error between the simulated and measured inclusions area percentage was for the case using $N = 1300$ and $D = 1.8$ mm. This case is plotted in Figure A2 and the simulation results are 97% too high and 60% too low for the bottom- and feeder-filled castings, respectively.

The simulated average inclusion diameter results are given in Figure A3. These compare consistently better for both gating cases, with and without gating, than the inclusion area percentage results. With gating, the simulation result for the mean diameter for parameters $N = 1300$ and mean inlet inclusion diameter $D = 1.8$ mm is within 0.08 mm of the measurement in Figure A3(a). Without gating, the same model parameters give the simulation average diameter 0.75 mm below the measurement in Figure A3(b). By preselecting the mean inclusion diameter at the inlet in the dross model, the mean inclusion indication size in the model results can be “calibrated” to be close to the measured size. The unavoidable shortcoming found in using the dross model in this case study was that there were too many inclusions on the casting cope surface for the bottom-filled castings, and not enough on the cope surface of the feeder-filled castings.

A summary table for the dross inclusion simulation and measurement results for the inclusion the case study castings is given in Table A1. This table can be compared with the air entrainment inclusion model results in Tables 1 to 3. In Table A1, the simulation parameters are given for each case; the number of inclusions entering the inlet (N) and the mean diameter of the inclusions (D) of the indications. The results in the table are the inclusion area percentage, inclusion count and inclusion mean diameter on cope surface for the case with gating are given in Table A1(a) and for the case with the casting filled through the feeder in Table A1(b).

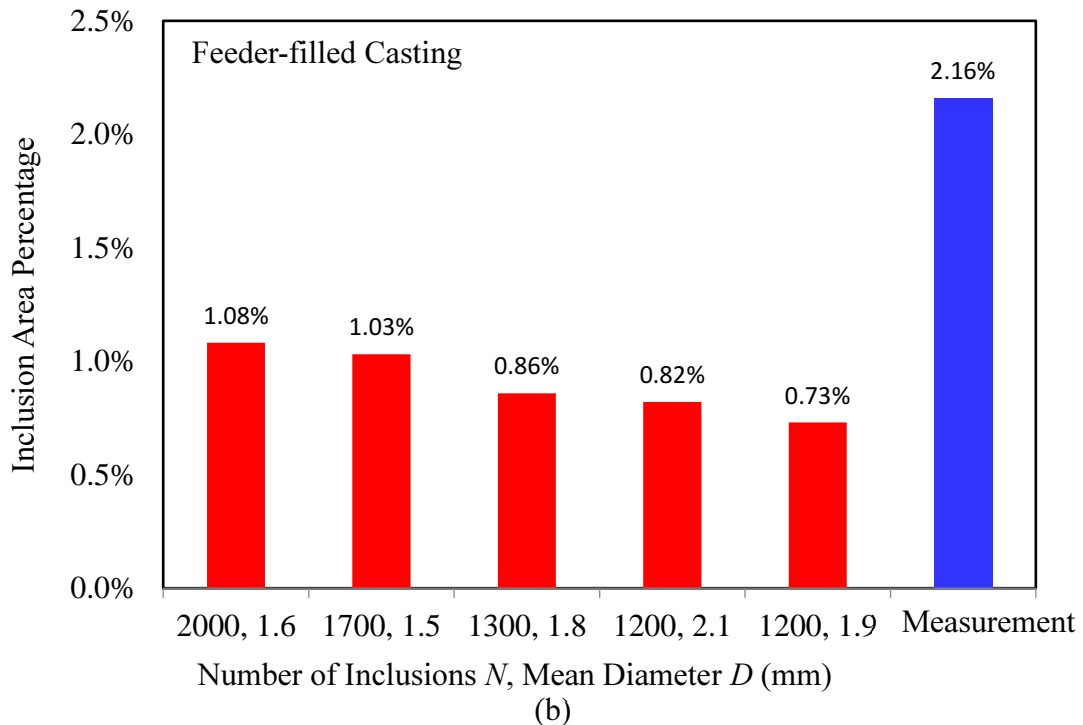
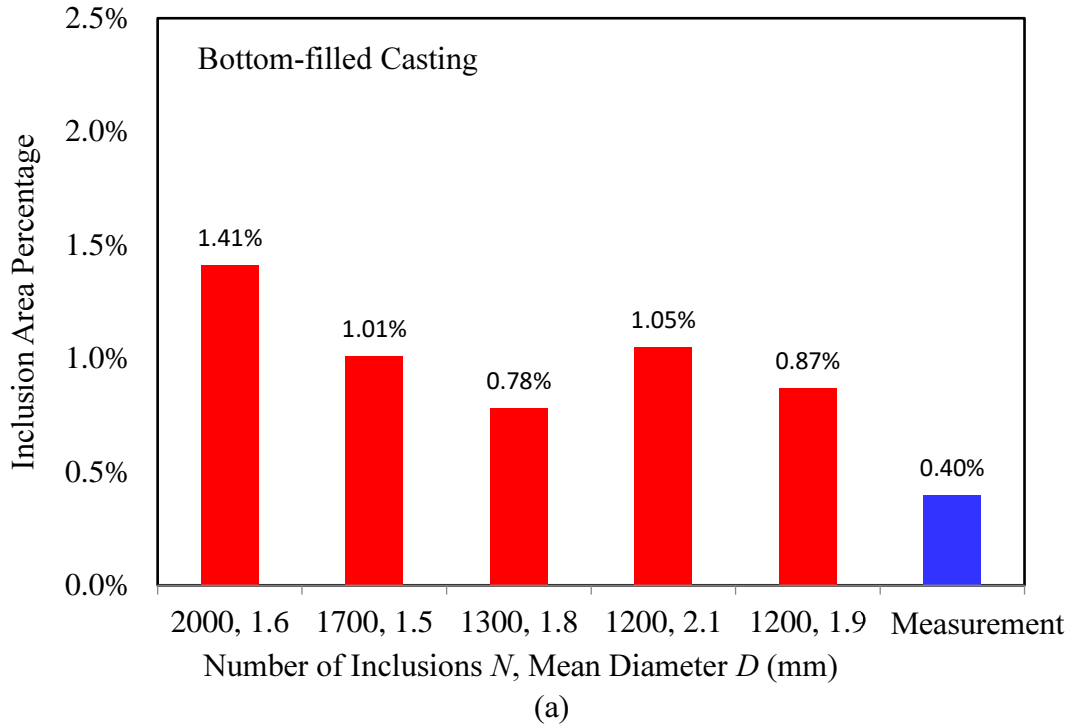


Figure A2. Inclusion area percentage results on the cope surface for measurements (blue bars), and simulations (red bars) with inclusion number at the inlet (N) ranging 1200 to 2000 and mean diameter of inclusions entering the inlet (D) ranging from 1.5 to 2.1 mm. Results are for case study casting with gating (a) and the case for casting filled through the feeder (b).

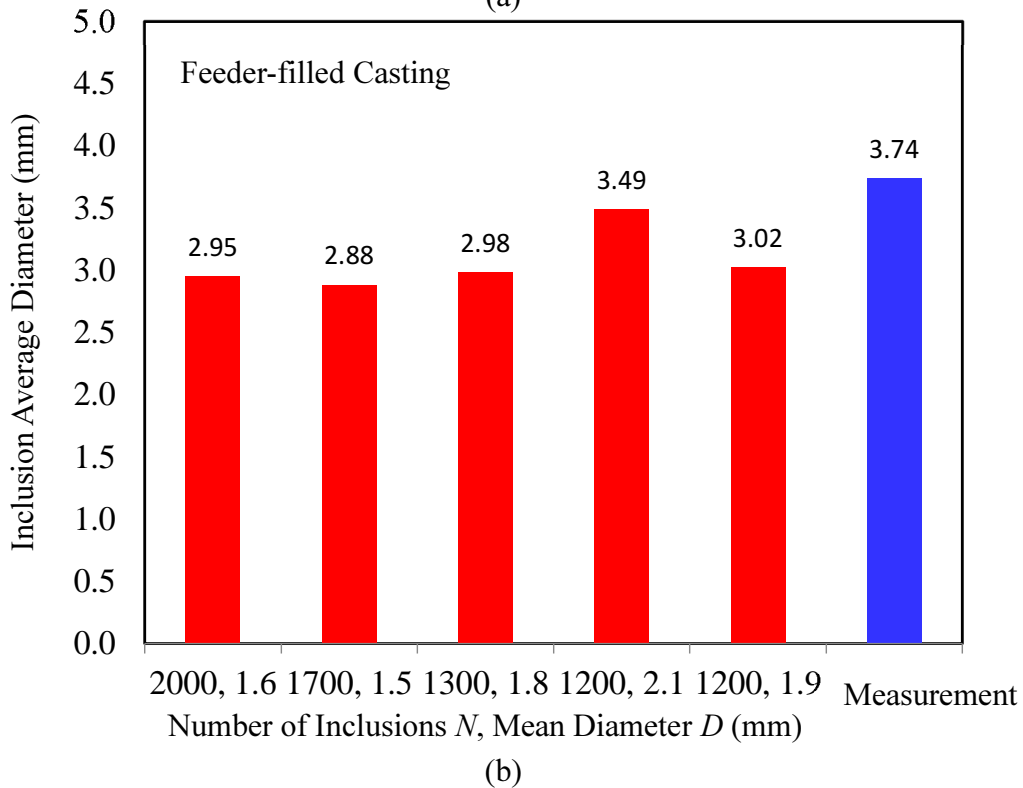
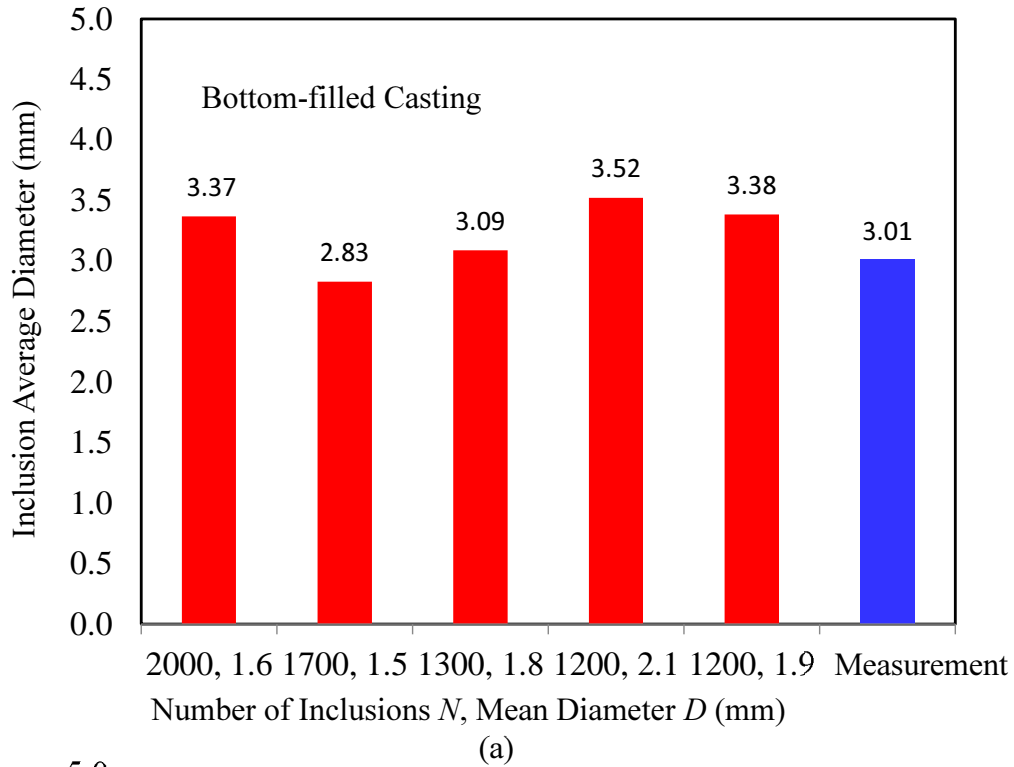


Figure A3. Inclusion indication average diameter results on the cope surface for measurements (blue bars), and simulations (red bars) with inclusion number at the inlet (N) ranging 1200 to 2000 and mean diameter of inclusions entering the inlet (D) ranging from 1.5 to 2.1 mm. Results are for case study casting with gating (a) and the case for casting filled through the feeder (b).

Table A1. Summary tables for cross model simulation and measurement results. The simulation parameters are given for each case; the number of inclusions entering inlet (N) and the mean diameter of the inclusions (D) of the indications. Measured and simulated results are shown for the case with gating (a) and case without gating (b).

(a)

Simulation Cases with Gating	Area %	Count	Mean Diameter (mm)
N=2000, D=1.58	1.41%	144	3.37
N=1700, D=1.5	1.01%	150	2.83
N=1300, D=1.8	0.78%	100	3.09
N=1200, D=2.1	1.05%	102	3.52
N=1200, D=1.9	0.87%	90	3.38
Measurement with Gating (%)	0.40%	37	3.01

(b)

Simulation Cases without Gating	Area %	Count	Mean Diameter (mm)
N=2000, D=1.58	1.08%	159	2.95
N=1700, D=1.5	1.03%	156	2.88
N=1300, D=1.8	0.86%	124	2.98
N=1200, D=2.1	0.82%	85	3.49
N=1200, D=1.9	0.73%	97	3.02
Measurement without Gating (%)	2.16%	100	3.74